Influences on Chemical Distribution Patterns across the west Greenland Shelf: The Roles of Ocean Currents, Sea Ice Melt, and Freshwater Runoff

Claudia E. Schmidt^{1,2}, Tristan Zimmermann³, Katarzyna Koziorowska⁴, Daniel Pröfrock³, Helmuth Thomas^{1,2}

¹Helmholtz-Zentrum Hereon, Institute of Carbon Cycles, 21502, Geesthacht, Germany

Correspondence to: Helmuth Thomas (helmuth.thomas@hereon.de)

30

Abstract The west Greenland shelf is a dynamic marine environment influenced by various physicochemical and biological processes. This study provides a comprehensivean overview of the main factors affecting the distribution of macronutrients, carbonate system parameters, and dissolved trace elements during Julylate summer. Key drivers include major ocean currents, melting sea ice, and terrestrial freshwater runoff, each contributing uniquely contributing to the cycling and spatial distribution of chemical constituents. Major ocean currents, such as the southward-moving Baffin Island Current (BIC) and the northwardmoving West Greenland Current (WGC), introduce water masses with distinct chemical signatures that shape the chemical composition of shelf waters by introducing water masses with distinct chemical signatures. Melting sea ice is serves as an important source of freshwater and dissolved constituents for the marine environment. The east to west direction of sea ice retreat creates nutrient gradients, with low nutrient levels in highly productive shelf waters and high nutrient levels in areas with prolonged ice cover. During the study period, we were able to capture a distinct nutrient gradient following the east-towest direction of sea ice retreat, with low nutrient levels in highly productive shelf waters and high nutrient levels in areas with prolonged ice cover. This process also affects influenced the carbonate system, leading to changes in pH and aragonite saturation states, which is critical tofer the health of marine organisms. Terrestrial freshwater runoff, particularly from the Greenland Ice Sheet (GIS), replenishes macronutrients in the photic zone, stimulating primary production and creating important CO₂ sinks. However, coastal surface waters become more susceptible to acidification by the input of poorly buffered glacial freshwater. Understanding these key drivers is essential for forecasting predicting future changes in the marine chemistry and ecosystem dynamics on biology of the west Greenland shelf, especially in the context of ongoing climate change within this high-latitude region.

²Carl von Ossietzky University Oldenburg, Institute for Chemistry and Biology of the Marine Environment, 26129, Oldenburg, Germany

³Helmholtz-Zentrum Hereon, Institute of Coastal Environmental Chemistry, 21502, Geesthacht, Germany

⁴Institute of Oceanology Polish Academy of Sciences, Department of Marine Chemistry and Biochemistry, 81-712, Sopot, Poland

1 Introduction

35

40

50

The physical system of the Arctic Ocean is inevitably changing, with profound implications for primary productivity (PP) and the biogeochemical cycling of nutrients and carbon across continental shelveson shelves and in-deep basins (Juranek, 2022). The complex coastal current system that connects the continental shelves of Greenland with the Arctic Ocean, the North Atlantic Ocean, and the Pacific Ocean strongly impacts PP (Vernet et al., 2021), creating an important environment for biota and fisheries (Krawczyk et al., 2021). The major ocean currents on the west side of Greenland are shown in Fig. 1 a. The circulation across the west Greenland shelf and Baffin Bay is dominated by the opposing direction of the Baffin Island Current (BIC) and West Greenland Current (WGC) (Curry et al., 2011). The circulation across the west Greenland shelf and Baffin Bay is dominated by two major currents in the region: the southward-flowing Baffin Island Current (BIC) along the Baffin Island continental slope and the northward-flowing West Greenland Current (WGC) along the west Greenland continental slope (Rysgaard et al., 2020). On the western side of Baffin Bay, the surface-intensified BIC transports water from the Alaskan shelf and the western Beaufort Sea through the narrow and shallow channels of the Canadian Arctic Archipelago (CAA), including- Nares Strait, Jones Sound, and Lancaster Sound, across Davis Strait into the Labrador Sea-(Nares Strait, Jones Sound, and Lancaster Sound) (Aksenov et al., 2016; Curry et al., 2011; Tang et al., 2004). Arctic waters of Pacific origin that entering Baffin Bay through the CAA have been identified as sources of described to be a source of dissolved trace elements (e.g., dMn, dFe, dCu, dNi) (Colombo et al., 2020; Colombo et al., 2021; Jensen et al., 2022) as well asand carbon (Azetsu-Scott et al., 2010; Burgers et al., 2024; Shadwick et al., 2011b). Further south, Davis Strait has been suggested acts as a gateway for the transport export of dissolved trace elements (Krisch et al., 2022a) and dissolved inorganic nitrogen (Juranek, 2022) from the Arctic to the North Atlantic Ocean. On the eastern side of Baffin Bay, the West Greenland Current (WGC) flows northward across Davis Strait and consists of the warm and low-salinity West Greenland Coastal Current (WGCC) on the shelf and the warm and high-salinity West Greenland Slope Current (WGSC) (Curry et al., 2011). These currents transport \(\pi_{\text{w}}\) atters of North Atlantic origin, which have been associated with anthropogenically elevated concentrations of dissolved lead (dPb) concentrations (Colombo et al., 2019), as well as enhanced but also higher biological productivity and species richness across the west Greenland shelf waters (Krawczyk et al., 2021). In the last two decades, sea ice concentrations in Baffin Bay and the Labrador Sea have decreased significantly due to climate change (Krawczyk et al., 2021). In the last two decades, sea ice concentrations in Baffin Bay and the Labrador Sea have declined significantly due to climate change (Krawczyk et al., 2021), additionally driven by an earlier melt onset and delayed freeze-up (Stroeve and Notz, 2018; Ballinger et al., 2022). Reduced sea ice cover has been correlated with an overall increase in productivity and species richness along the west Greenland shelf (Krawczyk et al., 2021; Møller et al., 2023). The reduction in sea ice cover, combined with increased inflow of Atlantic-sourced waters (Krawczyk et al., 2021) and elevated freshwater discharge (Møller et al., 2023), has been associated with an overall increase in PP and species richness along the west Greenland shelf (Krawczyk et al., 2021; Møller et al., 2023). In all seasonally ice-covered areas, intense but short-lived phytoplankton blooms develop in low-salinity waters at the edge of melting and retreating sea ice from spring to late summer

(Niebauer et al., 1995; Perrette et al., 2011). Phytoplankton growth is triggered by the stabilizing effect of sea ice meltwater-65 induced stratification in surface waters and the increased solar irradiance as the ice cover shrinks (Strass and Nöthig, 1996; Perrette et al., 2011). The newly exposed waters are initially still nutrient-rich but become rapidly depleted quickly become depleted aftefollowing the onset of the bloom (Niebauer et al., 1995). This is why In early summer, macronutrient distributions (NOx = nitrate + nitrate + nitrate) phosphate, PO_4^{3-} ; silicate, $Si(OH)_4$) in surface waters of Baffin Bay decrease along a west-to-east gradient, as they generally following the sea ice coverage (Lafond et al., 2019; Tremblay et al., 2002). Although sea ice meltwater is considered a negligible net source of macronutrients, it can significantly enhance trace element concentrations in the receiving waters (Evans and Nishioka, 2019; Hölemann et al., 1999; Kanna et al., 2014; Tovar-Sánchez et al., 2010). Elevated trace element concentrations in Arctic sea ice have been linked to entrained sediments (Measures, 1999) or atmospheric deposition from continuous emissions in highly industrialized countries (McConnell and Edwards, 2008). The carbonate system of Baffin Bay is influenced by sea ice meltwater, as it has the potential to supply additional alkalinity (AT) 75 (Jones et al., 1983). The carbonate system of Baffin Bay is influenced by sea ice meltwater, which has the potential to increase alkalinity (AT) relative to salinity. When the effect of salinity is removed, sea ice meltwater has been shown to supply additional AT in the form of buffering ions such as [CO₃²⁻] (Jones et al., 1983; Fransson et al., 2023). During sea ice formation, ikaite (CaCO₃ · 6H₂O) precipitates within the sea ice and is reintroduced to the water column during ice melt. This dissolution process resultsing in higher AT concentrations relative to dissolved inorganic carbon (CT), lower pCO_2 conditions, and higher pH as well as and argonite saturation state (Ω Aragonite) in surface waters (Fransson et al., 2013; Rysgaard et al., 2011; Rysgaard et al., 2012). However, on an annual cycle, sea ice does not serve as a net source or sink of these species to the underlying seawater. Instead, it serves as a mechanism for temporal and spatial redistribution, as these species are trapped during ice formation in autumn and winter, and subsequently released during ice melt – potentially at a different location due to drifting sea ice (Thomas et al., 2011). 85

The mass loss of the Greenland Ice Sheet (GIS) has increased sixfold since the 1980s, with the region northwards of Davis Strait experiencing the largest mass loss (Mouginot et al., 2019; Wouters and Sasgen, 2022). The export of glacial runoff from the GIS alters shelf and slope waters significantly, thus impacting PP in near coastal regions (Hawkings et al., 2015; Juul-Pedersen et al., 2015). The export of glacial runoff from the GIS alters the delivery of solutes and nutrients to near coastal regions (Hawkings et al., 2015) and the continental shelf (Cape et al., 2019). Thise glacier-derived freshwater alters marine concentrations of macronutrients (Hawkings et al., 2015; Hawkings et al., 2016; Hawkings et al., 2017; Hendry et al., 2019) and dissolved trace elements (Bhatia et al., 2013; Hawkings et al., 2020; Krause et al., 2021), influences localimpacts the hydrography, and facilitates-promotes the upwelling of nutrient-rich deep waters (Meire et al., 2017; Juul-Pedersen et al., 2015). This fertilizes adjacent marine systems and promotes high levels of biological productivity (Bhatia et al., 2013; Hawkings et al., 2020; Oksman et al., 2022). These processes enhance marine production and a prolonged annual productive season (Oksman et al., 2022). However, glacial freshwater is characterized by Glacial freshwater exhibits low AT and carbonate ion concentration (CO₃²⁻) relative to marine waters, thereby reducing the capacity of glacially modified waters to resist changes in pH driven by from the uptake of atmospheric CO₂ uptake (Bates and Mathis, 2009; Chierici and Fransson, 2009; Fransson

et al., 2015). In surface waters of Along the Greenlandic coast, AT dilution from glacial meltwater has been observed to drive corrosive conditions in surface waters, resulting in with an overall decreased in Ω Aragonite and pH (Henson et al., 2023; Shadwick et al., 2013). Photosynthetic CO₂ uptake can <u>partially</u> mitigate this negative effect of AT dilution, as PP reduces CT and pCO2 concentrations in surface waters and increases the carbonate saturation state (Chierici and Fransson, 2009; Hopwood et al., 2020; Meire et al., 2015).

In this study, we present recent (July 2021) measurements (July 2021) of the marine carbonate system, along with nutrient concentrations and dissolved (d; < 0.45 μ m) trace element concentrations across the west Greenland shelf in southern Baffin Bay between 64°N and 71°N (Fig. 1 b). Given the above considerations, the objectives of this study are to: (a) understand the physicochemical processes that influence the internal cycling of chemical constituents within the distinctin the different water masses of the shelf waters; and (b) resolve the regional and spatial differences in the distribution patterns on the west Greenland shelf during late summer that are driven by (i) major ocean currents, (ii) melting sea ice, and (iii) terrestrial freshwater runoff.

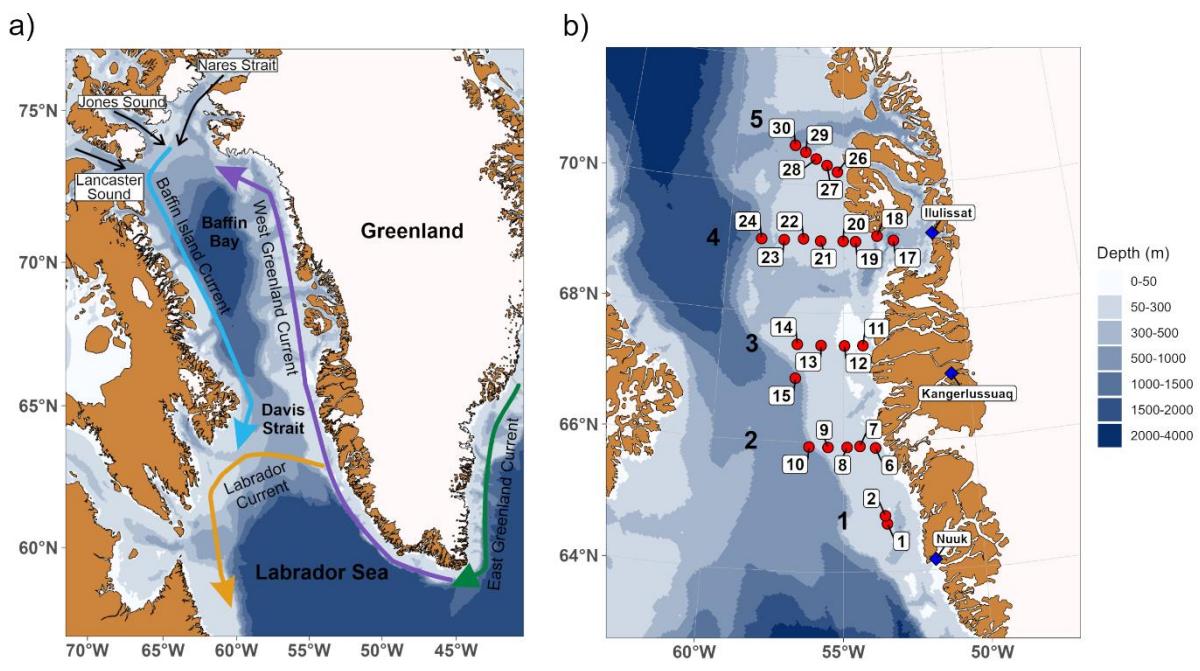


Figure 1: a) Schematic overview of the ocean currents and bathymetry in Baffin Bay and Davis Strait. Colored lines with arrows indicate the direction of different ocean currents. Bathymetry data from the GEBCO 2023 grid (GEBCO Bathymetric Compilation Group 2023, 2023). b) Map of the study area during DANA 6/21 with red points indicating the sampling locations and their affiliation to a certain transect (1-5).

2 Material and Methods

2.1 Study Area

100

105

110

115

A map of the study area with stations indicated by red dots is given in Fig. 1 b. General information about the selected stations and samples used in this study is provided in Table S 1. Samples were taken along two transects to the south and three transects

to the north of Davis Strait along the west Greenland shelf. Transect 1 was located in a shallow area (< 120 m depth) north of Nuuk. Transects 2 and 3 started close to the mouth of Kangerlussuaq Fjord and Nassuttooq Fjord, respectively. Station 15, which is part of transect 3, had to be moved further south because of the presence of sea ice. Transect 4 started in Disko Bay approximately 70 km from the mouth of the Ilulissat Icefjord, where the Jakobshavn Isbræ terminates. Transects 2, 3, and 4 continued westward away from the coast towards the shelf edge. Transect 5 started close to Disko Island and continued towards the northwest.

125 **2.2 Sampling**

Water column samples were taken at 25 stations as conductivity-temperature-depth (CTD) casts along five transects during ten consecutive sampling days between 18 and 28 July 2021 on board RV *Dana* (DANA 6/21, Fig. 1 b, Table S 1). A SBE 911 CTD+ unit (Sea-Bird Scientific; Bellevue, USA) was used to collect hydrographic profiles, including temperature, salinity, pressure, and dissolved oxygen. Two oxygen sensors were part of the CTD system and were calibrated prior to the cruise. By cross-referencing the data of the two sensors, we were able to monitor their drift during the cruise and correct the data accordingly. Samples were collected in 10 L metal-free Niskin water samplers (Ocean Test Equipment; Fort Lauderdale, USA). Detailed information about each sample is given in Table S 1, with sample IDs corresponding to the respective station and sampling depth.

2.2.1 Macronutrients

140

145

Water samples for nutrient analysis were collected in acid-washed 100 mL HDPE (high-density polyethylene) bottles. The bottles were preconditioned three times with sample water before being filled. The samples were stored frozen at -20°C without filtration until analysis.

2.2.2 Dissolved trace elements

Bulk samples for multi-element analysis were filled into acid-cleaned 2 L HDPE bottles. The bottles were rinsed three times with sample water before being filled. Immediately after sampling, the water samples were filtered as duplicates using high-purity, metal-free PFA (Perfluoroalkoxy alkane) filtration bombs (Savillex, Eden Prairie, USA) pressurized with nitrogen 5.0 (Air Liquide Danmark; Taastrup, Denmark) and acid-washed polycarbonate filters (0.45 µm, 47 mm diameter, Whatman, UK) in a clean bench (Erlab; Val de Reuil Cedex, France). More information about the filtration procedure can be found in Przibilla *et al.* (2023). The filtered samples were collected in pre-cleaned 250 mL HDPE bottles and stabilized using trace metal grade HCl (Fisher Scientific; Waltham, USA) before storage and shipping.

2.2.3 Carbonate system parameters

Samples for AT and CT were collected in 300 mL BOD (biological oxygen demand) bottles (Environmental Express, Charleston, USA) with an addition of 300 µL saturated mercury chloride solution (Carl Roth, Karlsruhe, Germany). The bottles

were sealed with ground-glass stoppers (Wheaton Science Products, New Jersey, USA), silicone- and halogen-free grease (type M, Apiezon, Manchester, UK), and plastic caps (Wheaton Science Products, New Jersey, USA), leaving no headspace. The samples were stored in darkness at ambient temperature until analysis.

2.3 Sample preparation and chemical analysis

2.3.1 Macronutrients

Nitrite, phosphate, and silicate were measured on a SmartChem 200 discrete analyser (AMS Alliance, Rome, Italy) following the reagent concentrations for the manual method in Hansen and Koroleff (1999), with the inclusion of a 150 g L⁻¹ solution of sodium dodecylsulfate as a dispersant for phosphate analysis. Nitrate was measured following the vanadium chloride reduction technique described by Schnetger and Lehners (2014). Community reference material for nutrients in seawater supplied by Kanso Technos Co. LTD, Japan, was used for quality control.

2.3.2 Dissolved trace elements

All equipment for trace metal analysis was acid-washed prior to use and rinsed with type I reagent-grade water (resistivity: 18.2 MΩ·cm) obtained from a Milli-Q Integral water purification system (Merck; Darmstadt, Germany) to prevent contamination. Dissolved trace elements (dV, dFe, dMn, dCo, dNi, dCu, dCd, and dPb) in seawater were measured with a seaFAST SP2 system (Elemental Scientific; Omaha, USA) coupled online to an inductively coupled plasma mass spectrometer (ICP-MS) (Agilent 7900, Agilent Technologies; Tokyo, Japan). The seaFAST SP2 system contained two columns filled with Nobias chelate-PA1 resin (HITACHI High-Tech Fielding Corporation; Tokyo, Japan). Detailed operating parameters and instrument configurations are given in Table S 2. More information about the analytical procedure can be found in Ebeling *et al.* (2022). For method validation, the certified reference material (CRM) NASS 7 (National Research Council Canada; Ottawa, Canada) as well as an in-house reference material (KBA-QC) mixed from single element standards (Carl Roth GmbH, Karlsruhe, Germany or Sigma-Aldrich, Missouri, USA) and custom-made multi-element standards (all traceable to NIST standards) of different compositions (Inorganic Ventures, Christiansburg, USA) were used. Recovery rates (between 97 % and 119 %) are given in Table S 3.

2.3.3 Carbonate system parameters

Measurements of AT and CT were performed using a VINDTA 3 C system (Marianda; Kiel, Germany). AT and CT were determined simultaneously by potentiometric titration using an 800 Dosino (Metrohm; Filderstadt, Germany) with an Aquatrode plus (Metrohm; Filderstadt, Germany) and coulometric titration using a CM5017O coulometer (UIC; Illinois, USA), respectively. Both instruments were calibrated against seawater CRMs (Scripps Institution of Oceanography; San Diego, USA) to ensure a precision of $\pm 1 \mu mol \ kg^{-1}$ for each parameter.

2.4 Data analysis

180

195

200

205

The raw CTD data were processed and averaged into 0.5 dbar pressure bins. The processed CTD data were used to construct water depth profiles of potential temperature, salinity, potential density, and oxygen (Fig. S 1 to S 5). Calculations were performed using R (version 4.2.2; (R Core Team, 2022)) and RStudio (version 2023.06.0; (Posit team, 2023)). Bivariate, linear data interpolation in combination with a surface approximation using multilevel B-splines with the "interp" function (package akima; (Akima and Gebhardt, 2022)) and the "mba.surf" function (package MBA; (Finley et al., 2022)) was used before plotting.

For trace elements analysis, filtration duplicates were obtained and measured as triplicates (n = 6). Outliers were identified using a Dean-Dixon outliers test and removed from further analysis. Mean concentrations (μ) and standard deviation (SD; σ) were estimated, considering twice the SD to represent $\mu \pm 2\sigma$. Limits of detection (LOD) and limits of quantification (LOQ) are given in Table S 3 and were calculated according to DIN 32645:2008-11 by measuring filtrations blanks (n = 8), with LOD defined as $3 \times SD$ and LOQ as $10 \times SD$ of the blank (DIN e.V., 2008).

The sum parameter NOx for nitrate and nitrite (NOx = nitrate + nitrite) was established and used throughout the discussion. The LOQs for the nutrient analysis are given in Table S 3.

Parameters of the carbonate system (pH, pCO₂, Revelle factor, and Ω Aragonite) were calculated using the CO2Sys Macro (Pierrot et al., 2011) with salinity, temperature, AT and CT as input variables. As input parameters, we used the dissociation constant by Mehrbach et al. (1973), refit by Dickson and Millero (1987), the HSO4- dissociation constant by Dickson (1990) and the seawater pH-scale (Dickson, 1990; Dickson and Millero, 1987; Mehrbach et al., 1973). We used the CO2Sys Macro to calculate temperature-normalized CT (CT_{temp}) according to Wu *et al.* (2019). The calculation was based on the median potential temperature of WGSW (3.23°C, n = 465) from the CTD profiles, filtered forwithin a depth range of 30 to 50 m₂. Further input parameters were using observed salinity, and the in situ pCO₂ as input parameters.

For statistical analysis, the data of the different parameters were merged according to station and sampling depth, obtaining one data matrix with 17 parameters and 41 observations. Values below LOD were replaced with a random value between zero and LOD. Each parameter was tested for normality (Shapiro-Wilk test, $\alpha = 0.01$) and transformed (log- or Box Coxtransformation) if the normality criteria was not met (Table S 4). The data were standardized, and principal component analysis (PCA) with varimax rotation was performed using the "principal" function (package psych; (Revelle, 2024)). Three principal components (PCs) were selected, considering the Guttman-Kaiser criterion and the trend of the scree plot. A broken stick analysis was performed to distinguish the loading significance of each variable.

3 Results

The distributions of basic oceanographic parameters (salinity, potential temperature, oxygen, apparent oxygen utilization (AOU)), macronutrients (NOx, silicate, phosphate), carbonate system parameters (AT, CT, pH, pCO₂, Revelle factor, Q Aragonite), and dissolved trace elements (dV, dMn, dFe, dCo, dNi, dCu, dCd, and dPb) are presented in separate sections.

The supplementary material (Fig. S 1 to Fig. S 12) provides detailed information on water column profiles and surface water concentration plots for individual parameters. Minimum and maximum values of macronutrients, carbonate system parameters, and trace elements are presented in Table 1. Figure 2 illustrates section plots for transect 4, highlighting a subset of the analyzed parameters.

215 Table 1: Minimum and maximum values of macronutrients, carbonate system parameters and trace elements across the study area.

	Unit	Minimum		Maximum		Literature data
Parameter		Value	Station	Value	Station [Depth in m]	Min – Max range
			[Depth in m]			
NOx	μmol L ⁻¹	0.21	13 [30]	17.85	15 [667]	2015: 0.032 – 24.3 1
1,011	milioi 2	V. - 1	10 [00]	17.00	10 [007]	2016: 0.05 – 28.5 ²
Silicate	μmol L ⁻¹	0.51	22 [3]	35.95	15 [667]	2015: 0.32 – 103.7 1
Silicate	μποι Ε	0.51	22 [3]	33.73		2016: 0.11 – 131.4 ²
Phosphate	μmol L ⁻¹	0.12	22 [3]	1.43	15 [667]	2015: 0.46 – 1.97 1
rnospiiate	μποι L	0.12	22 [3]	1.43	13 [007]	2016: 0.06 – 2.2 ²
AT	μmol kg ⁻¹	2062	15 [3]	2305	10 [551]	2015: 2156 - 2294 ⁴
AI						2016: 2176 – 2310 ³
CT	μmol kg ⁻¹	1949	15 [3]	2214	15 [667]	2015:2008-2255 ⁴
CT						2016: 1937 – 2277 ³
CT:AT		0.907	17 [3]	0.968	15 [667]	NA
pН		7.86	15 [667]	8.20	15 [32]	$2015: 7.40 - 7.81^{\ 1}$
$p\mathrm{CO}_2$	μatm	249	15 [32]	559	15 [667]	NA
Revelle factor		11.85	17 [3]	17.80	15 [667]	NA
Ω Aragonite		0.90	15 [667]	2.17	17 [3]	NA
dV	ng L-1	1270 ± 30	24 [3]	1810 ± 60	10 [551]	NA
dMn	ng L-1	54.8 ± 1.8	24 [317]	503 ± 20	12 [37]	$13.5 \pm 1.7 - 306.0 \pm 2.6$ ¹
dFe	ng L-1	56.9 ± 2.5	27 [15]	630 ± 30	18 [256]	$20.0 \pm 0.6 - 112 \pm 8^{\ 1}$
dCo	ng L ⁻¹	3.81 ± 0.15	10 [551]	14.7 ± 0.6	11 [3]	NA
dNi	ng L ⁻¹	232 ± 7	6 [3]	381 ± 4	24 [35]	$240 \pm 12 - 376 \pm 5^{-1}$
dCu	ng L-1	85.4 ± 2.5	10 [551]	206 ± 3	24 [3]	$115 \pm 10 - 333.0 \pm 0.7^{-1}$
dCd	ng L ⁻¹	3.1 ± 0.7	8 [4]	52.2 ± 1.2	15 [667]	$20.0 \pm 0.5 - 49.0 \pm 0.6$ ¹
dPb	ng L-1	0.99 ± 0.08	28 [186]	4.04 ± 0.13	10 [551]	$0.52 - 6.0^{\ 1}$

Note. The measurement uncertainty of trace elements corresponds to twice the SD with $\mu \pm 2\sigma$. Literature data from Geotraces cruise GN02 in 2015 (station BB1, BB2 and BB3) and GreenEdge cruise in 2016 (stations G100 to G3000). ¹(GEOTRACES Intermediate Data Product Group, 2023). ²(Bruyant et al., 2022). ³(Miller et al., 2020). ⁴(H. Thomas, personal communication, June 28, 2024).

220 **3.1 Basic oceanographic parameters**

225

230

235

240

The distribution of salinity, potential temperature, potential density, and oxygen are shown as water depth profiles for each transect in Fig. S 1 to 5. Due to Because of the high resolution of the CTD data, we give ranges of minimum and maximum values for salinity, potential temperature, oxygen and AOU are summarized in Table S 5. Salinity values were was generally the lowest in surface waters atof stations close to the coast (stations 6, 11 and 17) and towards the west of each transect (stations 14, 15, 24, 29 and 30), ranging between 29.70 and 32.60 with a minimum value of 29.70 recorded at the surface of station 14. The highest salinity (34.89) was observed in deep waters at station 10, between 530 and 558 m depth. In the deep waters of station 10, the salinity was the highest with 34.88 over a depth range from 500 to 558 m. Potential temperature was highest in surface waters in the southeastern part of Davis Strait, particularly at transect 2 (stations 6, 7, 8, and 10), and at station 17 in Disko Bay. Lower potential temperatures were found further offshore in the northwestern part of Davis strait. The minimum potential temperature of -1.63 °C was recorded in intermediate waters (40-55 m) at station 30, while the maximum value of 6.7 °C occurred in surface waters at station 8. Minimum potential temperature values between -1.50 to -1.61 °C were reached in the intermediate waters (20 to 75 m) of stations 24 and 30. Maximum potential temperature values between 5.6 to 6.7°C were measured in surface waters of transect 2 (stations 6, 7, 8 and 10), and in surface waters of station 17 in Disko Bay. Overall, temperatures were higher in the southeast of Davis Strait along the west Greenland coast and lower in the northwest of Davis Strait further offshore. In general, higher oxygen concentrations and lower AOU values were found in the photic zone (1.5–40 m), either near the Greenlandic coast at the beginning of transects (stations 6 and 17) or at the western ends (stations 10, 14, 15, and 24). The lowest oxygen concentration (204 µmol L⁻¹) and highest AOU (147 µmol L⁻¹) were observed in deep waters at station 15 (645 to 673 m). Conversely, the highest oxygen concentration (406 µmol L⁻¹) and lowest AOU (-72 µmol L⁻¹) were measured in intermediate waters (34 to 37 m) at station 10. In the deep waters of station 15, minimum oxygen concentrations between 203 to 210 µmol L⁻¹ and maximum AOU values between 140 to 147 µmol L⁻¹ were present over a depth range from 640 to 667 m. Maximum oxygen concentrations between 355 to 406 µmol L⁴ and minimum AOU values between 26 to 72 umol L⁻¹ were measured in the photic zone (1.5 to 40 m) either close to the Greenlandic coast at the beginning of a transect (stations 6 and 17) or towards the west of each transect (stations 10, 14, 15 and 24).

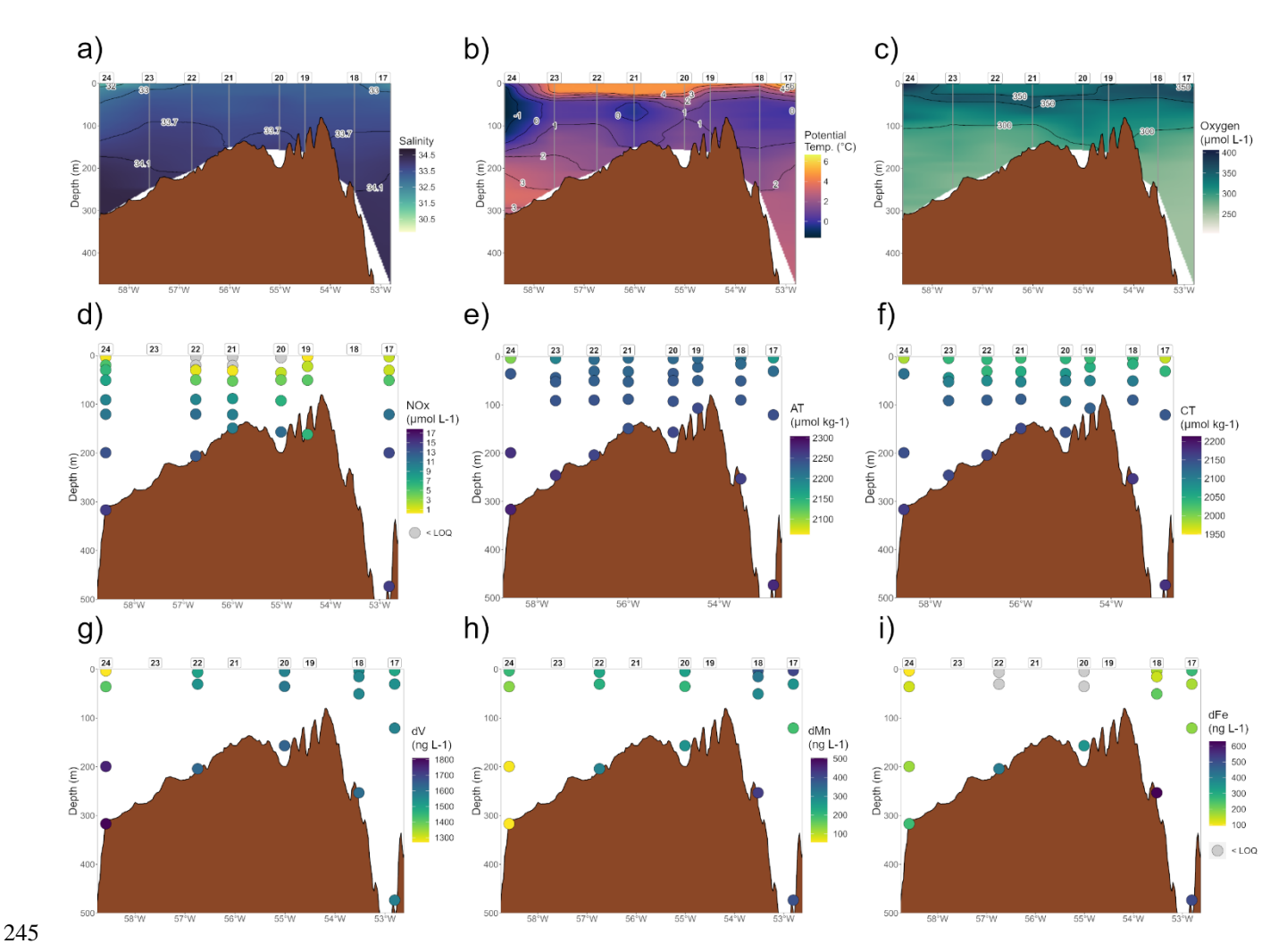


Figure 2: Section plots of transect 4 for selected parameters. Figures a) to c) present interpolated profiles of the water column derived from CTD data, illustrating the spatial distribution of key oceanographic parameters. Figures d) to i) depict the concentrations of specific parameters at various depths, providing detailed insights into the vertical structure and variability within the water column.

3.2 Macronutrients

The overall nutrient distribution is shown as vertical profiles in Fig. S 6 and as sea surface concentration plots in Fig. S 7. In surface waters, nutrient concentrations were uniformly low across the shelf. As illustrated in Fig. 2 d, Especially NOx concentrations were particularly low (< LOQ = 0.21 μmol L⁻¹) was extremely low in surface waters and shallow shelf waters. Exceptions to this trend were observed at station 17 in Disko Bay and at stations 14, 15, 24 and 30 towards the west of each transect, where are surface waters with higher nutrient concentrations were present at station 17 in Disko Bay and at stations 14, 15, 24 and 30 towards the west of each transect. Below the biological productive zone, nutrient concentrations gradually

increased with depth, reaching maximum concentrations at station 15 (667 m) (refer to Table 1). Sherwood et al. (2021) reported similarly high nutrient concentrations in these deep waters, which are further discussed in Sect. 4.1.2.

In comparison to data collected during 2015 (GEOTRACES Intermediate Data Product Group, 2023) and 2016 (Bruyant et al., 2022), maximum nutrient concentrations of this study are lower, which we attribute to regional differences in the study areas, especially referring to the maximum sampling depth. We measured maximum values at the shelf edge at 667 m, whereas the references reported maximum values at stations <u>located in central more central to</u> Baffin Bay-, where sampling extended to significantly greater depths in much greater depths.

3.3 Dissolved trace elements

260

265

275

280

The distributions of trace elements are shown as vertical profiles in Fig. S 8 and surface water concentrations in Fig. S 9. The section plots of dV, dMn and dFe are shown in Fig. 2 g to i. The vertical profiles of dV and dCu showed opposing trends (refer to Fig. S 8 a and f). With depth, dV concentrations increased, while dCu concentrations decreased. The dV concentrations ranged from 1270 ± 30 ng L⁻¹ (station 24; 3 m) to 1810 ± 60 ng L⁻¹ (station 10; 551 m), while dCu concentrations ranged from 206 ± 3 ng L⁻¹ (station 24; 3 m) to 85.4 ± 2.5 ng L⁻¹ (station 10; 551 m), both matching minimum and maximum occurrences of salinity. Surface waters close to the coast of Greenland and at the western end of each transect showed lower dV concentrations (Fig. 2 g and Fig. S 9 a) and higher dCu concentrations (Fig. S 9 f), respectively. The distributions of dFe, dNi and dCd showed low concentrations in surface and subsurface waters, which gradually increased with depth (refer to Fig. 2 i and Fig. S 8 c, e and g), reaching maximum concentrations for dFe of 630 ± 30 ng L⁻¹ (station 18; 256 m), for dNi of 307 ± 9 ng L⁻¹ (station 15; 667 m) and for dCd of 52.2 ± 1.2 ng L⁻¹ (station 15; 667 m). Minimum concentrations of dFe, dNi and dCd were present in surface waters (refer to Table 1) of stations with some distance to the coast, with dFe concentrations below the LOO (< 50 ng L⁻¹) at certain stations (Fig. 2 i). The concentration of dFe and dNi in surface waters (Fig. S 9 c and e) followed a similar pattern as the surface water nutrient concentrations (Fig. S 7). The concentrations were higher close to the coast, decreased with distance along each transect and increased again towards the west of each transect. The surface water concentrations of dCd were rather uniform and increased only towards the west of each transect (Fig. S 9 g). The concentration of dFe and dNi in surface waters (Fig. S 9 c and e) were higher close to the coast, decreased with distance along each transect and increased again towards the west of each transect. The surface water concentrations of dCd were rather uniform across the shelf and increased only towards the west of each transect (Fig. S 9 g). The concentrations of dMn and dCo decreased from surface to subsurface waters and increased again with depth at stations located on the shelf (refer to Fig. 2 h and Fig. S 8 b and d). On the shelf edge, concentrations of dMn and dCo remained stable with depth, leading to minimum concentrations for dMn of 54.8 ± 1.8 ng L⁻¹ (station 24; 317 m) and for dCo of 3.81 ± 0.15 ng L⁻¹ (station 10; 551 m). In surface waters, high concentrations of dMn and dCo were present at station 17 in Disko Bay (Fig. 2 h) and at stations 11 and 12, where the mouth of the Nassuttooq Fjord is located (Fig. S 9 b and d). The dMn and dCo concentrations in surface waters decreased with increasing distance from the coast. The depth profile of dPb does not follow a clear pattern (refer to Fig. S 8 h). South of Davis Strait, high dPb concentrations were observed across transect 2, alongside a maximum dPb concentration of 4.04 ± 0.13 ng L

¹ in the deep waters of station 10. North of Davis Strait, dPb concentrations were below the LOQ ($< 0.98 \text{ ng L}^{-1}$) in the deep waters of station 15, intermediate to deep waters of Disko Bay (stations 17 and 18) and in deep waters of station 28, along with a minimum concentration of $1.1 \pm 0.4 \text{ ng L}^{-1}$ in deep waters of station 30.

In comparison to literature values, our results for trace element concentrations are in a similar range as data collected during the 2015 Geotraces cruise GN02 (GEOTRACES Intermediate Data Product Group, 2023). Variations of minimum and maximum values occur because of differences in sampling locations. While this study took place on the shelf, capturing the influence of coastal runoff as well as sea ice meltwater, the Geotraces cruise focused on stations off the shelf and further north in central Baffin Bay.

3.4 Carbonate system parameters

The vertical profiles of AT and CT (Fig. 2 e and f and Fig. S 10 a and b) show a gradual increase with depth. Minimum concentrations of AT and CT were present in the low-salinity surface waters of station 15 (AT: 2062 μ mol kg⁻¹; CT: 1949 μ mol kg⁻¹). While maximum CT concentrations of 2214 μ mol kg⁻¹ were observed in the deep waters of station 15, AT concentrations followed the salinity gradient, reaching a maximum value of 2305 μ mol kg⁻¹ in the deep waters of station 10. The vertical profiles of pH and pCO₂ (Fig. S 10 d and e) show opposing trends, with pH increasing and pCO₂ decreasing towards intermediate waters of the photic zone. Below the photic zone, pH decreases and pCO₂ increases gradually with depth. This led to a pH maximum (8.20) and pCO₂ minimum (249 μ atm) in the photic zone of station 15 at 32 m, as well as minimum pH values of 7.86 and maximum pCO₂ values of 559 μ atm in the deep waters of station 15. The vertical profiles of the CT:AT ratio, the Revelle factor and Ω Aragonite (Fig. S 10 c, f and g) show that these parameters remain relatively stable in the first 25 m of the water column and gradually increase (CT:AT ratio and Revelle factor) or decrease (Ω Aragonite). In the surface waters of Disko Bay (station 17; 3 m) a minimum CT:AT ratio of 0.907, together with a minimum Revelle factor of 11.85 and a maximum Ω Aragonite value of 2.17 were present. The maximum CT:AT ratio (0.968) was found in the deep waters of station 15, which coincides with a maximum Revelle factor of 17.80 and a minimum Ω Aragonite value of 0.90.

The surface water concentrations of the carbonate system parameters are given in Fig. S 11. In general, stations closest to the coast of Greenland showed lower AT and CT values that increased with distance to the coast. Following this trend, the pH in surface waters increased and pCO_2 values decreased with distance to the coast along each transect. The lower CT:AT ratios of coastal stations coincided with higher Revelle factors and lower Ω Aragonite values, reflecting the lower buffering capacity of coastal waters. An exception to this was the surface waters of Disko Bay (station 17; 3 m). Here, the CT:AT ratio reached a minimum (0.907), caused by low CT values of 1972 μ mol kg⁻¹, corresponding to low pCO_2 values of 255 μ atm. Coupled to this, the pH is high (8.19) and the Revelle factor low (11.85), indicating the higher buffering capacity of this water, which is also reflected by a maximum Ω Aragonite value of 2.17. In surface waters of coastal stations 6 and 11, higher CT:AT ratios (0.920 and 0.925) coincided with higher Revelle factors (12.8 and 13.3) and lower Ω Aragonite values (1.93 and 1.82), reflecting the lower buffering capacity of coastal waters. In contrast, the surface waters of Disko Bay (station 17; 3 m) had lower CT:AT ratios (0.907), caused by low CT values of 1972 μ mol kg⁻¹, corresponding to low pCO2 values of 255 μ atm.

Coupled to this, the pH is high (8.19) and the Revelle factor low (11.85), indicating the higher buffering capacity of this water, which is also reflected by a maximum Ω Aragonite value of 2.17. The westernmost surface waters of each transect showed lower AT and CT values with overall highest CT:AT ratios in surface waters. Consequently, pCO_2 values and Revelle factors followed this trend and were higher at these stations, whereas pH and Ω Aragonite values were lower.

In comparison to AT and CT data collected during 2015 (H. Thomas, personal communication, June 28, 2024) and 2016 (Miller et al., 2020), our results are in a similar range as previous studies, but with minimum values being slightly lower as we were able to capture the sea ice meltwater signal.

3.5 Characterization of water masses

325

330 The distribution of water masses along the west coast of Greenland has been the subject of considerable discussion over the past decades, leading to the development of multiple classification systems and a wide range of nomenclatures. In this study, we identify water masses in the region based on characteristic salinity and potential temperature ranges, as illustrated in Fig. 3 (black boxes; based on Tang et al., 2004; Curry et al., 2011, 2014; Sherwood et al., 2021). This terminology is consistently applied throughout the discussion. An updated perspective on the water masses off the west Greenland coast was provided by 335 Rysgaard et al. (2020), and these more recent classifications are included for comparison in Fig. 3 (orange labels). Water depth profiles displaying potential temperature, salinity, potential density, and oxygen along the transects are provided in Fig. S1 to S5. The West Greenland Shelf Water (WGSW; θ < 7°C; S < 34.1) was the dominant water mass in the study area, occurring in each transect across the shelf above a water depth of 200 m. The WGSW is also referred to as Southwest Greenland Coastal Water (CW), originating from the East Greenland Current and modified by freshwater input from Greenlandic glacial runoff. 340 The West Greenland Intermediate Water (WGIW; $\theta > 2^{\circ}$ C; S > 34.1) was present in deeper waters along the slope below 200 m. This water mass corresponds to the Subpolar Mode Water (SPMW), of which we identified a colder and less saline variant – the deep Subpolar Mode Water (dSPMW) - along the slope. Arctic Water (AW; $\theta \le 2^{\circ}$ C; S ≤ 33.7) was detected north of Davis Strait at transects 3, 4, and 5, forming an intermediate layer between WGSW and WGIW above 100 m on the western side of the transects. These cold, low-salinity water pockets are illustrated in Fig. S3 to S5. At transect 4, AW was 345 found at station 17 approximately 70 km off the coast of Greenland, extending into Disko Bay. The updated classification refers to this water mass as Baffin Bay Polar Water (BBPW), of which a diluted form was found west of transects 4 and 5. Transitional Water (TrW; $\theta \le 2^{\circ}$ C; S > 33.7) was primarily observed at transects 4 and 5 between 100 and 200 m, separating AW from WGIW (Fig. S 4 to S 5). At station 15, the waters below 300 m were defined as Baffin Bay Water (BBW; $\theta \le 2$, S > 34.1), a shallower extension of the Baffin Bay Deep Water, presenting as a distinct tail on the θ -S diagram (Sherwood et al., 2021). Due to very low surface salinity values at stations 14, 15, and 24 (S < 31.5), we introduced sea ice meltwater (SIM) 350

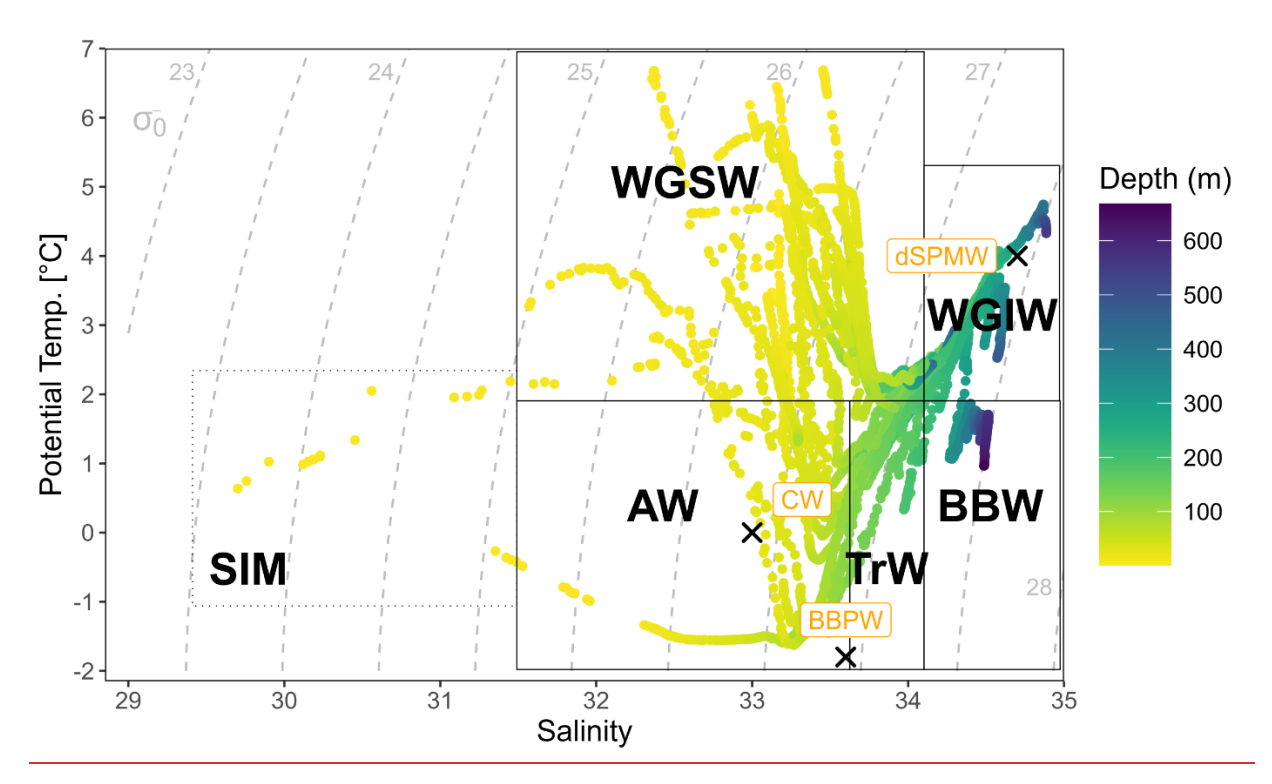


Figure 3: Water masses in the study area were characterized using potential temperature and salinity: West Greenland Shelf Water (WGSW; $\Theta < 7^{\circ}$ C; S < 34.1), West Greenland Intermediate Water (WGIW; $\Theta > 2^{\circ}$ C; S > 34.1), Transitional Water (TrW; $\Theta \le 2^{\circ}$ C; S > 33.7), Arctic Water (AW; $\Theta \le 2^{\circ}$ C; S ≤ 33.7) and Baffin Bay Water (BBW; $\Theta \le 2^{\circ}$ C, S > 34.1), according to Curry *et al.* (2011), Curry *et al.* (2014), Sherwood *et al.* (2021), and Tang *et al.* (2004). Surface water with S < 31.5 is indicative of sea ice meltwater (SIM). An updated perspective on the water masses was provided by Rysgaard et al. (2020): Baffin Bay Polar Water (BBPW; $\Theta = -1.8^{\circ}$ C, S = 33.6), Southwest Greenland Coastal Water (CW; $\Theta = 0^{\circ}$ C, S = 33), and deep Subpolar Mode Water (dSPMW; $\Theta = 4^{\circ}$ C, S = 34.7).

4 Discussion

355

360

365

4.1 Characterization of water masses

4.1.1 Temperature-salinity properties

The water masses along the west Greenland shelf were identified using salinity and potential temperature (Curry et al., 2014; Tang et al., 2004; Curry et al., 2011; Sherwood et al., 2021) as shown in Fig. 2. Water depth profiles displaying potential temperature, salinity, potential density, and oxygen along the transects are provided in Fig. S1 to S5. The West Greenland Shelf Water (WGSW; $\theta < 7^{\circ}$ C; S < 34.1) was the dominant water mass in the study area, occurring in each transect across the

shelf above a water depth of 200 m. The West Greenland Intermediate Water (WGIW; $\theta > 2^{\circ}\text{C}$; S > 34.1) was present in deeper waters along the slope below 200 m. Arctic Water (AW; $\theta \le 2^{\circ}\text{C}$; $S \le 33.7$) was encountered north of Davis Strait at transects 3, 4, and 5 as an interlayer between WGSW and WGIW above 100 m on the west side of the transects, forming cold and low-salinity pockets of water (Fig. S 3 to S 5). At transect 4, AW was found at station 17 approximately 70 km off the coast of Greenland, reaching far into Disko Bay. Transitional Water (TrW; $\theta \le 2^{\circ}\text{C}$; S > 33.7) was present mainly at transects 4 and 5 between 100 and 200 m, separating AW from WGIW (Fig. S 4 to S 5). At station 15, the waters below 300 m were defined as Baffin Bay Water (BBW; $\theta \le 2$, S > 34.1), a shallower extension of the Baffin Bay Deep Water, presenting as a distinct tail on the θ S diagram (Sherwood et al., 2021). Due to very low surface salinity values at stations 14, 15, and 24 (S < 31.5), we introduced sea ice meltwater (SIM) as an additional source water to distinguish areas affected by sea ice melt.

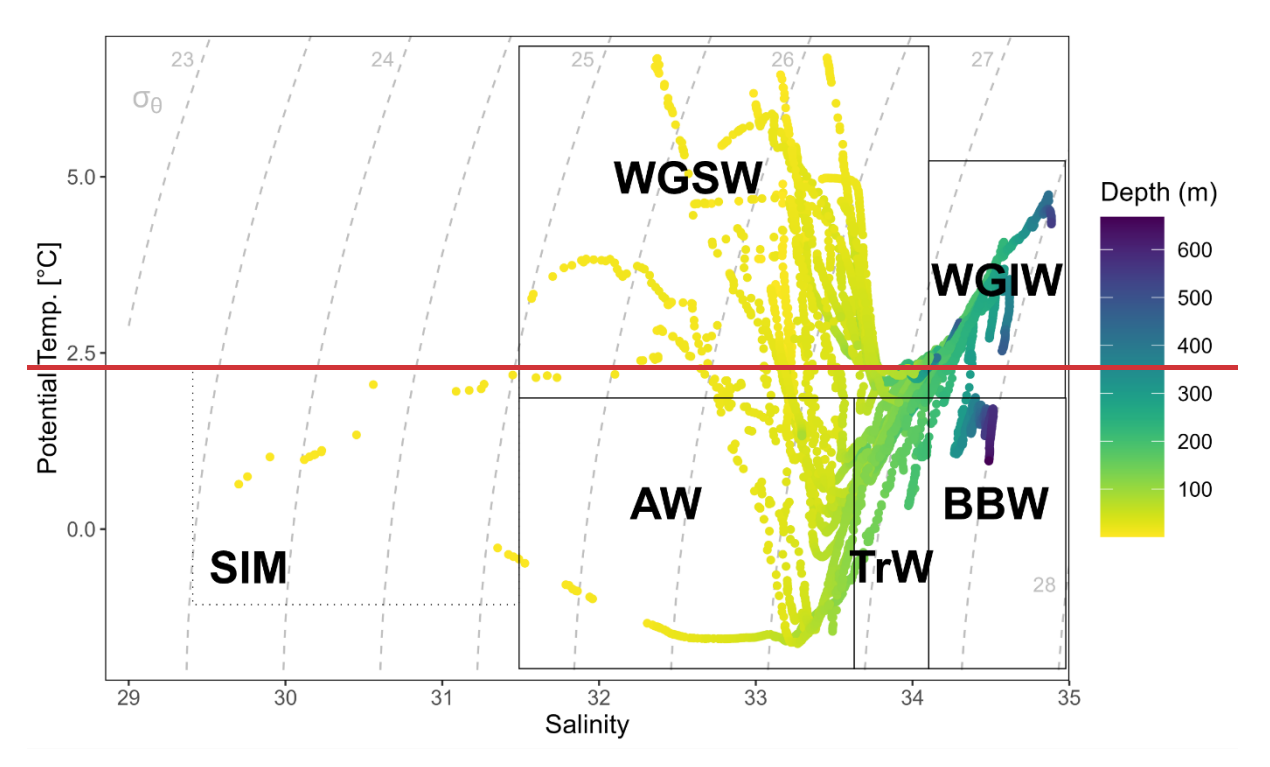


Figure 3: Water masses in the study area were characterized using potential temperature and salinity: West Greenland Shelf Water (WGSW; $O < 7^{\circ}C$; S < 34.1), West Greenland Intermediate Water (WGIW; $O > 2^{\circ}C$; S > 34.1), Transitional Water (TrW; $O \le 2^{\circ}C$; S > 33.7), Arctic Water (AW; $O \le 2^{\circ}C$; $S \le 33.7$) and Baffin Bay Water (BBW; $O \le 2$, S > 34.1), according to Curry et al. (2011), Curry et al. (2014), Sherwood et al. (2021), and Tang et al. (2004). Surface water with S < 31.5 is indicative of sea ice meltwater (SIM).

4.1.2 Influence of physicochemical processes on biogeochemical properties

370

375

380

385

The extensive data set was processed using PCA to further characterize the water masses and to find physicochemical processes that alter the distribution of carbon, macronutrients, and trace elements. The results of the PCA analysis are summarized in Table S 6, with significant PC loadings of each parameter marked in bold. Overall, 82 % of the total variance in the normalized

data set can be explained by three PCs. The majority of variance is explained by PC 1 with 52 %, followed by PC 2 with 18 % and PC 3 with 12 %. Salinity, depth, oxygen, AT, CT, dV, and dCu significantly load on PC 1; potential temperature, AOU, NOx, silicate, phosphate, dNi, dCd, and dPb significantly load on PC 2; and dFe, dMn, dCo, dNi, and dCu significantly load on PC 3. Figure 3 shows the results of the PCA as biplots with colors indicating the water mass affiliation of each sample.

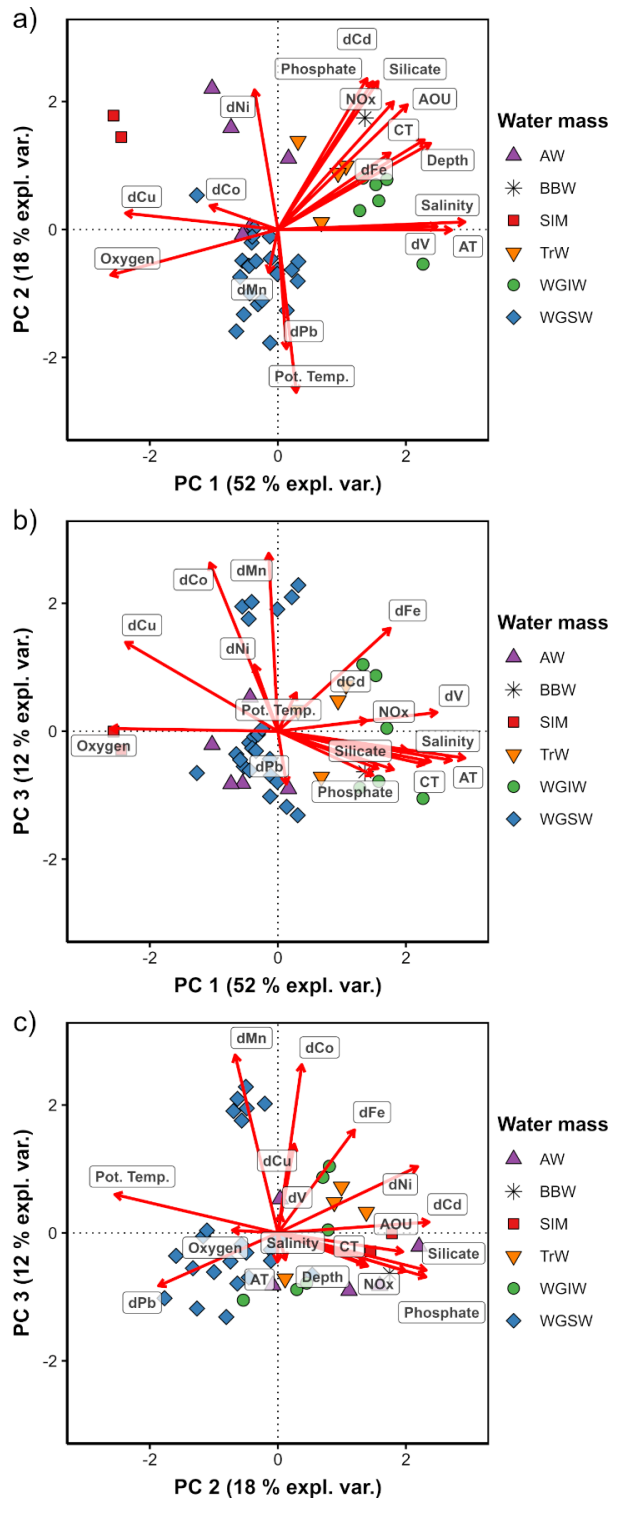


Figure 4: Biplots according to PCA results for a) PC 1 score vs PC 2 score; b) PC 1 score vs PC 3 score; and c) PC 2 score vs PC 3 score, with colors indicating the water mass affiliation of each sample. The loading of each parameter is indicated by a red arrow.

4.1.1 Conservative mixing along the salinity gradient (PC 1)

395

400

405

410

415

420

425

The comparison of low PC 1 scores of surface water samples with lower salinity (WGSW, AW, and SIM) and high PC 1 scores inof deeper, more saline water masses samples with higher salinity (WGIW, TrW, and BBW) indicates that PC 1 is resolvesing the salinity gradient of the study area (Fig. 43 a and b). The WGSW integrates freshwater contributions from the GIS (Foukal and Pickart, 2023), while AW represents a mixture of mixes winter-cooled water entering Baffin Bay on the eastern side of Davis Strait and with inflow of cold, and fresh Arctic Ocean water of Pacific origin flowing through the CAA (Curry et al., 2014). Melt water from sea iceSea ice meltwater promotes a fresh surface layer that tends to remains concentrated in the upper part of the water column (Haine et al., 2015).

The statistical results illustrate the importance of freshwater input on the chemical properties of the study area. The high loading of AT, CT, dV, and dCu on PC 1 indicates that these parameters behave conservatively, with freshwater being either being a source (dCu) or a cause for dilution (AT, CT, and dV) of parameter concentrations. The positive loadings of AT and CT on PC 1 are in lineconsistent with the general understanding that of freshwater inputs from sea ice meltwater and glacial meltwater, which are characterized by low AT and CT values concentrations (Bates and Mathis, 2009; Chierici and Fransson, 2009; Fransson et al., 2015). The positive correlations of AT and CT against salinity are illustrated in Fig. S 12 a and b. Similarly, The distribution of dV shows a positive correlation with salinity (Fig. S 12 c), as both sea ice melt and coastal freshwater inputs were characterized by are associated with low dV concentrations (Marsay et al., 2018; Whitmore et al., 2019). The distribution of dCu correlated negatively with salinity and was influenced by coastal freshwater input and sea ice meltwater as a dCu source (Fig. S 12 d). The distribution of dCu correlated negatively with salinity and was primarily influenced by coastal freshwater input (Fig. S12d). Sea ice meltwater also contributed to elevated dCu concentrations in surface waters (Fig. S9f), particularly toward the western ends of Transects 4 and 5. Cu-binding ligands play an important role in maintaining Cu in the dissolved phase (Ruacho et al., 2022), thereby facilitating and facilitate the transport of dCu across the Arctic (Arnone et al., 2023). This is reflected in the consistent <u>lateral</u> decrease of dCu concentrations in the <u>lateral direction</u> away from the coastal sources along the shelf transects (refer to Sect. 3.3). The influence of freshwater input on the chemical properties of the water column is further discussed in Sect. 4.4, regarding sea ice meltwater in Sect. 4.4 and in Sect. 4.5, which addresses coastal runoff in Sect. 4.5.

4.1.2 Biological uptake and recycling (PC 2)

The high positive loading of AOU, NOx, silicate, phosphate, dNi, and dCd on PC 2 suggests that PC 2 describes distributions that are controlleddriven by biological cycling. The nutrient-type behavior of dNi and dCd, was mentioned as discussed in Sect. 3.3, and agrees aligns well with the PCA results. In addition Additionally, dFe also shows a high loading on PC 2, reflecting its nutrient-type character. This observation is consistent This in good agreement with previously published data for the Nansen Basin and the Barents Sea (Gerringa et al., 2021), the Chukchi Sea (Vieira et al., 2019), the Fram Strait (Krisch et al., 2022a) and the Canadian Arctic (Colombo et al., 2020).

The anticorrelation between of nutrients (positive PC 2 loading) and potential temperature (negative PC 2 loading) reflects the spatial distribution derives from the distribution of theose parameters across the study area. LThe low PC 2 scores of WGSW indicate that the warmer shelf waters are highly productive, resulting in low nutrient concentrations. In contrast, Tthe colder deep waters of TrW, WGIW and BBW are characterized by exhibit high PC 2 scores, suggesting remineralization processes that return which implies that remineralization occurred with nutrients and trace elements being returned to the water column. Similarly, water samples of AW and SIM water samples also show high PC 2 scores, characterized by with higher nutrient concentrations alongside colder lower temperatures. The difference in nutrient concentrations between AW and WGSW is further discussed explored in Sect. 4.3, while and the influence of the retreating sea ice is discussed in Sect. 4.4.

The remineralization of organic matter (OM) led to elevated concentrations of NOx, silicate, phosphate, and dCd, together along with maximum AOU values (refer to Sect. 3.1 and 3.2) in the deep waters of BBW (640 to 667 m; station 15). Although we only encountered at this station, our results agree wellare consistent with Sherwood et al. (2021), who observed are ported similar trend with similar AOU and nutrient concentrations in BBW. The accumulation of Rremineralized nutrients accumulate at depth because of attributed to the long residence time of deep and bottom waters in Baffin Bay, in combination with the region's enclosed bathymetry, an enclosed bathymetry which that restricts circulation (Sherwood et al., 2021; Lehmann et al., 2019).

Besides nutrients In addition to nutrients, CT also has shows a high loading on PC 2, whereas while AT only loads exclusively on PC 1. This distinction highlights statistical feature illustrates the different biogeochemical behavior of AT and CT. While AT is primarily influenced distributions are dominated by freshwater dynamics, CT is also significantly affected distributions are also equally driven by biological processes. Consequently, This resulted in elevated CT concentrations were observed in BBW (refer to Sect. 3.4). Here, high CT values coincided with the, where restricted circulation and remineralization contribute to, which led to overall more corrosive conditions for the Baffin Bay shelf sediments and benthic ecosystems. Similar to other studies inof Baffin Bay (Beaupré-Laperrière et al., 2020; Burgers et al., 2024), OM respiration in deep waters led to undersaturation respiration of OM drove deep waters to become undersaturated with respect to Ω Aragonite, accompanied by increased pCO₂ and decreased pHwith pCO₂ increasing and pH decreasing proportionally to each other (refer to Sect. 3.4).

Alongside potential temperature, dPb has exhibited a negative loading on PC 2, reflecting a latitudinal trend in which stems from the latitudinal trend of potential temperature and dPb concentrations (refer to Sect. 3.1 and 3.3). The distribution of dPb is mainly-primarily controlled by the mixing of warm Atlantic-origin waters with high dPb signatures and cold Arctic-origin waters with low dPb signatures (Colombo et al., 2019). As a result, dPb concentrations were highestThis resulted in high dPb concentrations in the warmer waters southeast of Davis Strait, andwhich decreased progressively toward the colder northwesttowards the northwest as temperatures decreased.

4.1.3 Scavenging and benthic processes (PC 3)

430

435

440

445

450

455

The third PC <u>is</u> associate<u>ds</u> with the trace elements dMn, dFe, dCo, dNi, and dCu. It is known that during estuarine mixing, dCo, dNi and dCu are co-cycled with dMn and dFe throughduring their incorporation transformation into the respective

(oxy)hydroxide mineral_phases (Smrzka et al., 2019). We suggest that PC 3 indicates particle-driven mixing of these trace elements with coastal runoff as a source. High PC 3 scores (Fig. 43 b and c) of surface samples taken at from stations 11 and 12 (mouth of Nassuttooq Fjord) as well as station 17 (Disko Bay) highlight the dominant influence illustrate the prevailing role of coastal freshwater inputs on the distribution of these trace elements. The influence role of coastal runoff in shaping on trace element distribution is further discussed in Sect. 4.5.

The biplots (Fig. 43 b and c) reveal a notablean interesting feature of deep water samples (111 to 667 m), identified as TrW and WGIW. At these shelf stations, elevated concentrations of dMn, dFe, dCo, and dNi were observed in deep water samples concentrations of dMn, dFe, dCo, and dNi are increased (refer to Sect. 3.2), which we attribute to suggest is caused by benthic processes occurring in surface sediments, i.e., reversible scavenging linked to mineral dissolution and the remineralization of organic material. Benthic Release from the benthic boundary layer has been described for of dCo, dFe, and dMn has been documented in the Barents Sea (Gerringa et al., 2021), the Chukchi Sea (Vieira et al., 2019), the Canadian Arctic (Colombo et al., 2020) and throughout the Arctic basin (Bundy et al., 2020), while benthic dNi release has been reported and for dNi in the Bering Sea and Chukchi Sea (Jensen et al., 2022). In contrast, dCu did not exhibit signs of ashowed no benthic source or evidence of biological cycling, and iInstead, its distribution remained dominated by freshwater runoff from coastal sources, consistent with observations by similar to what has been observed by Jensen et al. (2022).

A striking feature of these deep shelf water samples is the divergence in PC3 scores: some stations (8, 10, 15, 24, 30) show negative scores, while others (17, 20, 22, 28) exhibit positive scores. Noticeable for these deep water shelf samples is a dissociation of corresponding PC 3 scores into negative scores (stations 8, 10, 15, 24, 30) and positive scores (stations 17, 20, 22, 28). We interpret this pattern as a reflection of spatial variability. We believe this division to be caused by differences in return fluxes at the sediment-water interface. Stations with a positive PC 3 scores are located closer to the coast, where greater export of biogenic and terrigenous material enhances recycling more biogenic and terrigenous material is exported, which can be recycled in deep waters. In contrast, offshore Sstations that are further away from the coast do not receive less particulate input, resulting in lower trace element concentrations and negative PC3 scores as much material for remineralization and have, thus, a negative PC 3 score with lower concentrations of the trace elements dMn, dFe, dCo and dNi. A similar pattern was observed by Seo et al. (2022) in the Ulleung Basin of the East Sea, where significantly higher concentrations of dMn, dFe, and dCo were found on the slopes and in the bottom layer compared to the Japan Basin. The authors attributed this to enhanced sedimentary release driven by the high organic matter content of shelf sediments (Seo et al., 2022). A similar observation was made for dMn, dFe, and dCo in the Ulleung Basin of the East Sea by Seo et al. (2022). Concentrations were significantly higher on the slopes and bottom layer of the Ulleung Basin in contrast to the Japan Basin, which the authors associated with a large sedimentary release by OM degradation caused by the high OM content of the shelf sediments (Seo et al., 2022).

4.23 Influence of major current systems on biogeochemical properties

465

470

475

480

485

490

The spatial distribution of parameters revealed significant differences in eastern and western shelf waters. <u>To investigate these</u> <u>differences</u>, we conducted a direct comparison of <u>We decided to directly compare</u> the three major water masses present along

the west Greenland shelf: the northward-moving WGSW (1 to 220 m) and WGIW (130 to 560 m) with the southward-moving AW (2 to 165 m). For each parameter, the median and the mean \pm SD values are summarized in Table 2. The median is used throughout the data discussion because of its robustness against outliers.

Table 2: Comparison of the median and mean \pm SD concentrations between WGSW, WGIW and AW. The number of samples (n) used for the calculation is given in brackets.

		WGSW	WGIW	AW
	Parameter	(Median;	(Median;	(Median;
		Mean \pm SD)	Mean \pm SD)	Mean \pm SD)
Basic oceanographic parameters	Salinity	33.57	34.45	33.48
(WGSW: $n = 3021$;	Samily	33.52 ± 0.42	34.45 ± 0.23	33.42 ± 0.27
WGIW: $n = 3034$;	Pot. Temp.	2.68	2.93	0.38
AW: $n = 2301$)	(°C)	3.20 ± 1.15	3.16 ± 0.73	0.15 ± 1.02
	Oxygen	336	273	332
	$(\mu mol L^{-1})$	344 ± 23	278 ± 21	332 ± 23
	AOU	-4	62	36
	(µmol L ⁻¹)	0 ± 26	55 ± 23	30 ± 24
Macronutrients	NOx	1.7	13.5	5.7
(WGSW: $n = 54$;	$(\mu mol L^{-1})$	2.4 ± 2.8	13.7 ± 1.7	6.0 ± 2.8
WGIW: $n = 9$;	Silicate	1.5	10.6	4.2
AW: $n = 29$)	$(\mu mol L^{-1})$	2.0 ± 1.8	11.5 ± 4.1	5.2 ± 3.5
	Phosphate	0.23	1.02	0.66
	$(\mu mol L^{-1})$	0.31 ± 0.18	0.99 ± 0.13	0.68 ± 0.21
Carbonate system parameters	AT (μmol kg ⁻¹)	2226	2275	2237
(WGSW: $n = 50$;	A1 (μιποι kg ⁻)	2228 ± 19	2278 ± 11	2237 ± 6
WGIW: $n = 12$;	CT (µmol kg ⁻¹)	2051	2164	2104
AW: $n = 25$)	C1 (µmor kg ')	2056 ± 28	2159 ± 16	2104 ± 27
	CT:AT	0.922	0.950	0.941
	CI:AI	0.923 ± 0.007	0.948 ± 0.006	0.941 ± 0.010
	all.	8.14	7.99	8.10
	pН	8.14 ± 0.03	7.99 ± 0.04	8.09 ± 0.06
	~CO (u -t)	292	433	321
	pCO_2 (µatm)	295 ± 22	$2 425 \pm 37 332 \pm 52$	
	O A	1.88	1.30	1.48
	Ω Aragonite	1.86 ± 0.15	1.34 ± 0.12	1.49 ± 0.20

Continuation of Table 2: Comparison of the median and mean \pm SD concentrations between WGSW, WGIW and AW. The number of samples (n) used for the calculation is given in brackets.

		WGSW	WGIW	AW	
	Parameter	(Median;	(Median;	(Median;	
		Mean \pm SD)	Mean \pm SD)	Mean \pm SD)	
Trace elements	dV (ng L ⁻¹)	1490	1735	1480	
(WGSW: $n = 31$;	dv (ng L ')	1486 ± 234	1713 ± 121	1478 ± 127	
WGIW: $n = 8$;	4E- (I-1)	116	262	162	
AW: $n = 8$)	dFe (ng L ⁻¹)	138 ± 67	329 ± 55	174 ± 26	
	D4 (x 1)	237	89	186	
	dMn (ng L ⁻¹)	261 ± 71	164 ± 13	184 ± 20	
	10 · (· · · I · l)	8.0	5.0	9.0	
	dCo (ng L ⁻¹)	8.5 ± 2.5	5.7 ± 0.5	9.2 ± 0.8	
	JNT' (T1)	254	269	266	
	dNi (ng L ⁻¹)	258 ± 51	270 ± 22	280 ± 20	
	10 (1-1)	161	111	160	
	dCu (ng L ⁻¹)	158 ± 44	111 ± 13	162 ± 16	
	101/ 11	13	31.6	21.6	
	dCd (ng L ⁻¹)	13 ± 6	32.2 ± 2.7	22.0 ± 2.3	
	1D1 (1-1)	2.4	2.4	1.7	
	dPb (ng L ⁻¹)	2.5 ± 0.8	2.4 ± 0.5	1.8 ± 0.4	

The median values of salinity and potential temperature reflect the origin of the water masses and the freshwater dynamics of this area. In the upper water column, AW is slightly fresher (33.48) and colder (0.38°C) than WGSW (33.57; 2.68°C). This east—west gradient in temperature and salinity haswas also been.described by Tang et al. (2004) between Baffin Island and the Greenland coast. AsWhen the warmer WGSW flows cyclonically around Baffin Bay and mixes with adjacent waters from of the CAA, itthe water becomes progressively colder and fresher, eventually.before returning as the southward <a href="https://example.colder.cold

The AOU concentrations are reflective of respiration and the biological activity of the water (Sarmiento and Gruber, 2006). Lower AOU values in WGSW (4 μmol L⁻¹) than in AW (36 μmol L⁻¹) indicate that the warmer shelf waters are more productive than the colder AW. As AOU is a depth-dependent variable, we propose examining a consistent depth range of 30 to 50 m to enable a more meaningful comparison between WGSW and AW. Within this range, the median AOU values are -6 μmol L⁻¹ for WGSW and 7 μmol L⁻¹ for AW. This suggests that warmer shelf waters (WGSW) are more biologically

productive than colder AW, as indicated by greater oxygen production in the upper water column. Although primary production was not directly measured in this study, this interpretation is supported by Krawczyk et al. (2021), who reported the highest chlorophyll a concentrations along the southwest Greenland coast and the lowest values along Baffin Island. This pattern is consistentis also in agreement with overall lower nutrient concentrations observed in WGSW than-compared to AW (refer to Sect. 4.1.2 and Table 2), as nutrients are removed from the water column through during PP. With depth, respiration returns nutrients to the water column as seen by high AOU values in WGIW (62 µmol L=1) and overall higher nutrient concentrations (refer to Table 2). Fig. 54 a shows the represents NOx concentrations plotted against longitude within the 30 to 50 m depth range in a depth range of 30 to 50 m, including literature data from the Green Edge cruise in 2016 (Bruyant et al., 2022). A clear spatial gradient is evident, with There is a clear difference between-lower NOx concentrations in WGSW on the shelf and higher NOx concentrations in AW further offshore, particularly in areas that were still ice-covered. This nutrient gradient in nutrient reflects the east-to-west progression of sea ice retreateoncentrations is caused by the direction of the sea ice retreat from east to west and has been linked to enhanced PPhigher productivity and species richness along the southern coast of west Greenland and in Disko Bay, compared to the more nutrient-rich but less productive regions near Baffin Island and northwest Greenland (Krawczyk et al., 2021; Lafond et al., 2019). We believe that our sampling near the end of the summer season was erucial for this vast difference in water mass composition. We consider the timing of our sampling during the mid-summer season to be critical in capturing the pronounced differences in water mass composition. By this time, sShelf waters had already become depleted in nutrients, whereas offshore regions were only beginning to experience increased biological processes following the retreat of sea icewhile further offshore biological processes only increased recently because of the retreating sea ice (refer to Sect. 4.4). With increasing depth, respiration returns nutrients to the water column, as evidencedseen by high AOU values in WGIW (62 umol L⁻¹) and overall higher nutrient concentrations at depth (refer to Table 2).

520

525

530

535

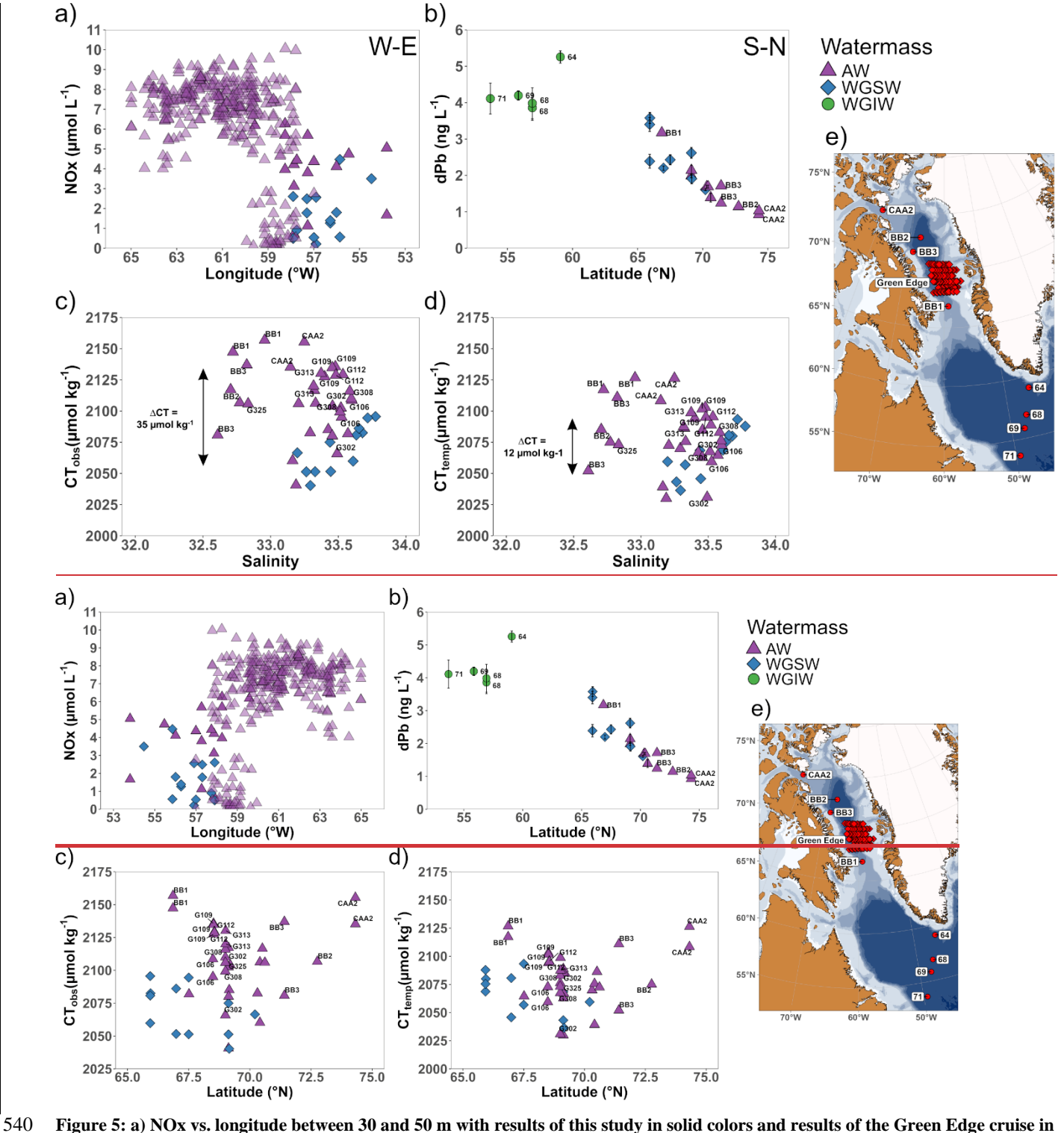


Figure 5: a) NOx vs. longitude between 30 and 50 m with results of this study in solid colors and results of the Green Edge cruise in transparent colors (Bruyant et al., 2022); b) dPb vs. latitude between 30 and 50 m with results of this study (unlabeled) in comparison

to results of the Geotraces GA01 cruise in 2014 (stations 64-71) and Geotraces GN02 in 2015 (BB1-BB3, CAA2), both: (GEOTRACES Intermediate Data Product Group, 2023); c) CT_{obs} and d) CT_{temp} vs. salinitylatitude between 30 and 50 m with results of this study (unlabeled) in comparison to results of the Green Edge cruise (Miller et al., 2020) and Geotraces GN02 in 2015 (BB1-BB3, CAA2) (H. Thomas, personal communication, June 28, 2024); e) location of the stations used as comparison. Different water mass categories are given in the legend.

545

550

555

560

565

570

A Ccomparison of the carbonate system parameters in WGSW and AW shows reveals that both AT and CT median concentrations were lower in WGSW. This observation alignseoincides well with a study by Burgers et al. (2024), whoich reported that described the dominant source of freshwater for eastern Baffin Bay isto be glacial meltwater, characterized by a significantly with a much lower AT endmember (390 ± 140 µmol kg⁻¹) compared to the western Baffin Bay, where with an the AT endmember isof 1170 ± 120 µmol kg⁻¹. The higher median CT:AT ratios in AW (0.941) compared to WGSW (0.922) isare attributed to caused by the inflow of relatively low --salinity Pacific-origin waters to western Baffin Bay, which exhibit elevated with higher CT:AT ratios., In contrast, while Atlantic waters transported to eastern Baffin Bay have with lower CT:AT ratios are transported to eastern Baffin Bay (Burgers et al., 2024). This carbon enrichment in AW can be traced back to the CAA outflow, which contains higher CT concentrations of Pacific-origin (Shadwick et al., 2011b; Azetsu-Scott et al., 2010). These slightly higher CT:AT ratios in AW than WGSW were are also reflected inby a higher median pCO₂ concentration, and lower median pH value and lower median Ω Aragonite concentration (refer to Table 2). To minimize depth-related variability, we further examined CT values within a consistent depth range of 30 to 50 m. For a more detailed discussion about CT values in AW and WGSW, we looked at a depth range of 30 to 50 m to eliminate any depth dependency. It is well established known that colder sea surface temperatures at high latitudes contribute significantly to explain the latitudinal gradient majority of their surface CT latitudinal gradient, due to the increased CO₂ solubility of colder waters (Wu et al., 2019; Li and Tsui, 1971). To assess the extent to which temperature differences between AW and WGSW influence CT concentrations, we calculated temperature-normalized CT (CT_{temp}) following the method described by Wu et al. (2019) (see Sect. 2.4). This normalization was based on the median potential temperature of WGSW (3.23 $^{\circ}$ C, n = 465) within the 30 to 50 m depth range. We examined the extent of the CT change induced by the temperature difference between AW and WGSW. Therefore, we calculated temperature normalized CT (CT_{temp}) according to Wu et al. (2019) (refer to Sect. 2.4.) based on the median potential temperature of WGSW (3.23°C) within a depth range of 30 to 50 m. The observed CT (CT_{obs}) and CT_{temp} values for AW and WGSW are shown in Fig. 54 c and d-for AW and WGSW. For comparison, wWe included literature data from the Green Edge cruise (Miller et al., 2020) and Geotraces GN02 in 2015 (BB1-BB3, CAA2) (H. Thomas, personal communication, June 28, 2024), filtered for ato the same depth range of 30 to 50 m. Including literature data, the difference between the median CT values of AW and WGSW is $\frac{ACT}{\Delta CT_{obs}^{WGSW-AW}} = 35 \,\mu \text{mol kg}^{-1}$. After temperature normalization, the difference is significantly reduced to $\Delta CT_{temp}^{WGSW-AW} = 12 \mu mol kg^{-1}$. This indicates that the majority Therefore, we conclude that most of the CT difference in AW and WGSW is induced driven by the temperature difference of both between the two water masses. The remaining CT difference may be attributed to could be caused by the higher biological productivity in WGSW, which lowers reduces CT concentrations, and tocombined with the mixing of AW and with the CAA outflow, which is known to transport additional CT to Baffin Bay (Shadwick et al., 2011b; Burgers et al., 2024; Azetsu-Scott et al., 2010).

<u>InTowards</u> the deeper waters of WGIW, <u>both</u> AT and CT median concentrations <u>were higherincrease</u>, as they increased <u>alongfollowing</u> the salinity gradient and <u>reflecting the contribution of OM</u> respiration <u>of OM-to the</u> released <u>of CT</u> to the water column. This is also <u>evidentreflected</u> in higher median pCO₂ concentrations and lower median Q Aragonite concentrations in WGIW (refer to Table 2), consistent with <u>similar to</u> observations by Burgers *et al.* (2024).

580

585

590

595

600

605

All median concentrations of trace elements exhibiting that showed a nutrient-type profile (dFe, dNi, and dCd) were are lower in WGSW than compared to AW. This difference is attributed to caused by their biological uptake during PP, which was higher in WGSW than AW. The return of these elements to the water column through the due to remineralization of OM is evidentean be seen in higher the elevated median concentrations observed in WGIW (refer to Table 2). In addition to biological cycling Furthermore, variations in source water composition also contribute concentrations could lead to differences in trace element concentrations. AW showed exhibited elevated concentrations for dFe, dMn, dCo, dNi, and (refer to Table 2). These higher concentrations are likely linked We attribute these high concentrations to the CAA outflow into Baffin Bay., This outflow has been shown which was found to have higher dFe and dMn concentrations eaused by due to sediment resuspension in the benthic boundary layer (Colombo et al., 2020; Colombo et al., 2021), as well as higher dNi and dCu concentrations associated with Pacific-origindue to waters advected from the Canada Basin through the CAA and out into Baffin Bay (Jensen et al., 2022). In contrast to other trace elements, higher dPb median concentrations were present observed in WGSW and WGIW compared tothan AW (refer to Table 2). As mentioned in Sect. 3.3, a latitudinal gradient in dPb concentrations exists across Davis Straitthere is a difference in dPb concentrations between the south and the north of Davis Strait, with dPb concentrations decreasing along the west coast of Greenland. This trend is illustrated in Fig. 5 b, where dPb concentrations are plotted against latitude within the 30 to 50 m depth range. The figure combines our data with literature values from the Geotraces GA01 cruise in 2014 (stations 64 to 71) and Geotraces GN02 in 2015 (BB1-BB3, CAA2), both: (GEOTRACES Intermediate Data Product Group, 2023). We illustrated this trend by plotting dPb against latitude in a depth range between 30 and 50 m (Fig. 4 b) as a combination of our results with literature data from the Geotraces GA01 cruise in 2014 (stations 64 to 71) and Geotraces GN02 in 2015 (BB1 BB3, CAA2), both: (GEOTRACES Intermediate Data Product Group, 2023). The elevated dPb concentrations in WGSW and WGIW are likely influenced by The results show that WGSW and WGIW entailed higher dPb concentrations, with freshwater input from the GIS (Krisch et al., 2022b) and North Atlantic waterswater from the North Atlantic (Colombo et al., 2019) being as a source of dPb, respectively. In contrast, AW contained exhibited much lower dPb concentrations, which we attribute to which we relate to low dPb concentrations in the CAA outflow, as this region is relatively remote isolated from anthropogenic inputs sources of dPb (Colombo et al., 2019). Our results demonstrate that the distribution of dPb is mainly primarily controlled by the mixing of water masses with different distinct dPb signatures. As such, dPb can serve as a useful tracer for illustrating the gradual mixing and transformation of water masses along the West Greenland shelf, and can be used to illustrate the gradual mixing of the three water masses along the shelf.

4.34 Influence of retreating sea ice on biogeochemical properties

610

615

620

625

Baffin Bay and its surrounding areas are generally-typically ice-free between July and October (Bi et al., 2019). Our The statistical analysis illustrated highlighted the importance significant influence of SIM on the chemical composition of surface waters (refer to Sect. 4.1.2). To visualize the decline in sea ice concentration during the sampling period, w\text{W} e used the ASI sea ice concentration product provided by the University of Bremen (Spreen et al., 2008) to visualize the decline in sea ice concentration over the sampling period. Figure 5 a shows illustrates the difference change in sea ice concentration between 19 July and 28 July 2021. At the beginning of our sampling period on 19 July 2021, two large extensive areas with high sea ice concentration were present between 66°N-68°N and 70°N-74°N. By 28 July 2021, These areas had disappeared almost completely by the end of our sampling period on 28 July 2021, indicating a rapid and complete sea ice retreat within just 10 daysthe complete melting of sea ice in the study area over 10 days. Thise melt event significantly affected sea surface salinity and potential temperature, depicted as shown in Fig. 65 b and c. Both parameters decreased towards the west along transects 3, 4 and 5, with salinity reaching a minimum of 29.70 (station 14; 3 m) and potential temperature of -0.36°C (station 24; 3 m). The category SIM (refer to Sect. 4.1) was identified in the top-upper 4 m of stations 14 and 24, and in the top-upper 8 m of station 15. Although not formally classified as SIM, a similar trend of decreasing reduced surface salinity and potential temperature values can be seenwas observed at stations 10, 13, 23, 28, 29, and 30, adjacent to SIM stations (Fig. S 2 to S 5). We suggest that this trend is caused by the reflects the gradual advection of SIM from Baffin Bay towards the southeast.

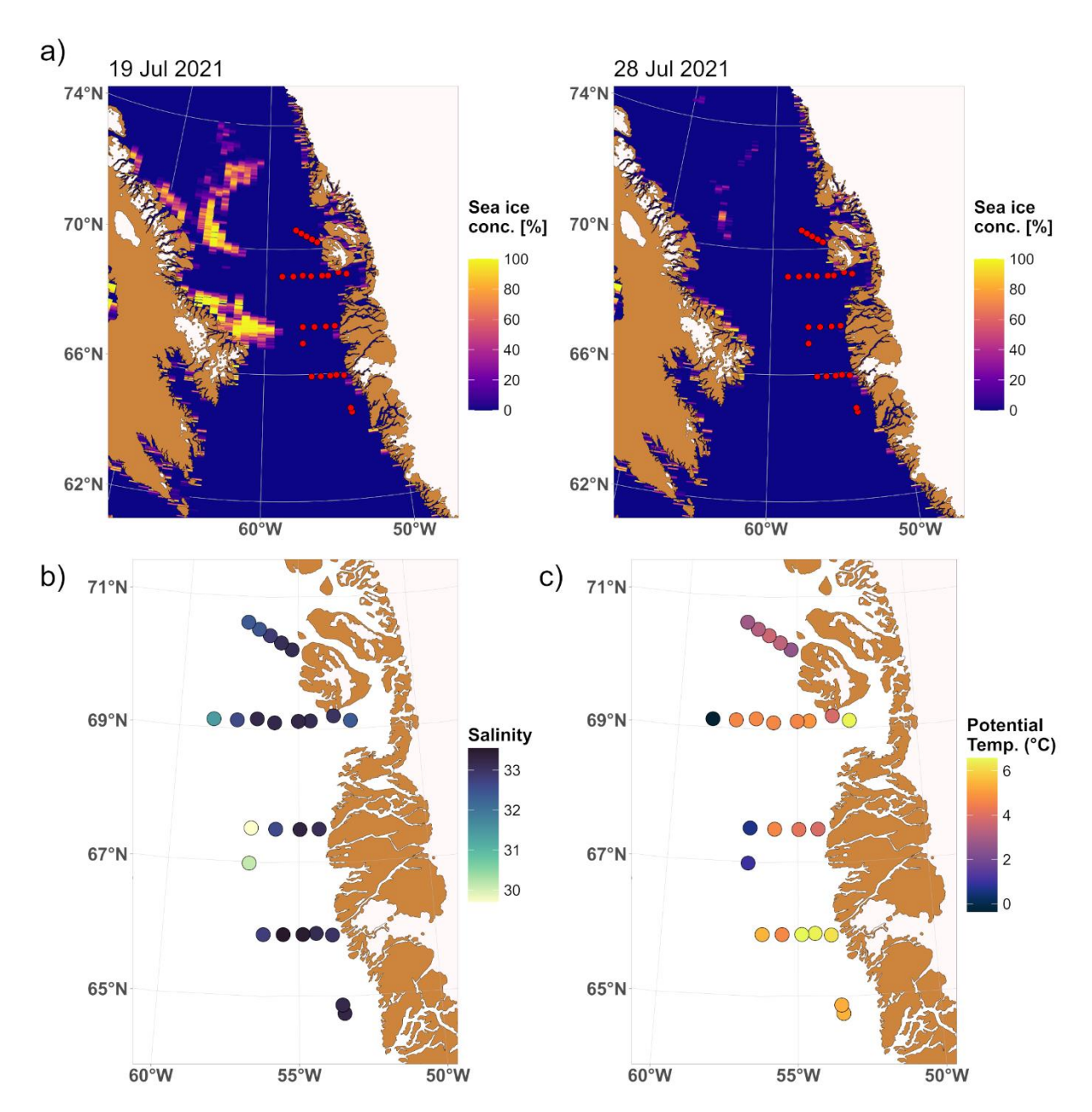


Figure 6: a) Sea ice concentration (%) in the study area during the sampling period on 19 July and 28 July 2021. Sea ice concentration data (ASI data, ASMR2, version 5.4, 3.125 km grid) was downloaded from the data archive of the University of Bremen (Spreen et al., 2008). Sea surface b) salinity and c) potential temperature from CTD sensor data.

Lafond *et al.* (2019) observed that stations covered by sea ice had higher surface nutrient concentrations than open-water stations located east of the ice edge, where nutrients were elose to depletion nearly depleted. In this study, the distribution of nutrients in surface waters surface nutrients follows a similar trend (refer to Sect. 3.2). Along each transect, nutrient concentrations were consistently higher towards the west, corresponding with the recent retreat of sea icefollowing the retreat

of the sea ice. High Elevated oxygen concentrations and low AOU values in these westerns areas (refer to Sect. 3.1) suggest the onset of a phytoplankton bloom that a phytoplankton bloom started to develop. The timing of the study enabled us to observe that nutrients had not yet been fully consumed in these western areas, whereas while shelf waters farther east had already become depleted due to earlier biological activity towards the east.

635

640

645

650

655

660

665

Our observations of the carbonate system show indicate that surface waters of stations affected influenced by SIM had exhibited lower AT and CT concentrations, with overallalong with higher CT:AT ratios., These conditions resulteding in higher pCO_2 values and lower Q Aragonite values (refer to Sect. 3.4). Similar results of sea ice meltwater increasing pCO_2 and decreasing CaCO₃ mineral saturation states have been described reported along the east and west coast of Greenland (Henson et al., 2023), the Fram Strait (Tynan et al., 2016), and in other Arctic regions but also in other parts of the Arctic such as the Canada Basin (Bates et al., 2009). To investigate the effect of sea ice on the first-upper 50 m of the water column, which is the typical penetration depth of sea ice meltwater (Jones et al., 1983), we calculated salinity-normalized AT (AT_{sal} = 35AT/S) and temperature-salinity-normalized CT ($CT_{temp}^{sal} = 35CT_{temp}/S$)₄ according to Wu et al. (2019) (refer to Sect. 2.4. and 4.3). These normalizations account for the effects of temperature and salinity on CO2 solubility, while remaining sensitive to biological processes, air–sea gas exchange, and water mass mixing We used normalized concentrations to account for temperature and salinity effects on the solubility of CO₂. The normalized concentrations remain dependent on biological processes, air sea gas exchange and mixing of water masses (Shadwick et al., 2011a). For AT_{sal} (Fig. 76 a), the majority of most surface water concentrations ranged between 2330 and 2350 μ mol kg⁻¹. We observed an AT addition in AT of ≈ 25 to 55 μ mol kg⁻¹ for SIM stations and of ≈ 5 to 45 µmol kg⁻¹ for SIM adjacent stations. These values are consistent Our results agree well-with Jones et al. (1983), who observed reported an AT addition of $\approx 100 \,\mu \text{mol kg}^{-1}$ further north in Baffin Bay, where sea ice meltwater influence is more pronouncedin a region that is more dominated by sea ice meltwater than our study area. This AT enrichment is attributed to the release of alkalinity during the melting of sea ice that contains ikaite, as described by Rysgaard et al. (2011, 2012) and Jones et al. (1983). The additional AT is released during melting of sea ice containing ikaite (Rysgaard et al., 2012; Rysgaard et al., 2011; Jones et al., 1983). The expected change increase in CT by ikaite dissolution should be one half the corresponding change in AT (Jones et al., 1983), or approximately 15 to 30 µmol kg⁻¹. The CT^{sal} values are shown in Fig. 76 b, with most surface water concentrations ranging between 2140 and 2170 μmol kg⁻¹. At SIM stations, There is we <u>observed</u> an addition in CT_{temp}^{sal} for SIM stations of ≈ 60 to 75 µmol kg⁻¹, and <u>at SIM adjacent stations</u> of ≈ 10 to 60 µmol kg⁻¹ for SIM adjacent stations. Hence, the observed CT addition exceed the expected contributionis much higher than what is expected from ikaite dissolution alone. Possible explanations for this high surplus in CT could be the release of CT derived from organic carbon remineralization under the ice (Tynan et al., 2016; Bates et al., 2009) and the inflow of additional CT transported through the CAA to Baffin Bay (Shadwick et al., 2011b; Henson et al., 2023; Azetsu Scott et al., 2010). Possible explanations for the observed surplus in CT include the release of CT from organic carbon remineralization under the ice (Tynan et al., 2016; Bates et al., 2009), or within the ice itself, as sea ice is known to contain higher concentrations in OM than the underlying seawater (Vancoppenolle et al., 2013). Additionally, the inflow of CT-enriched waters transported through the CAA into Baffin Bay may contribute to the elevated CT levels (Shadwick et al., 2011b; Henson et al., 2023; Azetsu-Scott et al., 2010). Our results show indicate that the dissolution of ikaite in sea ice acted as a source of AT, providing a small geochemical buffer to surface waters influenced by meltwatermeltwater influenced surface waters (Jones et al., 2021). However, the inflow of Pacific-origin waters and remineralization under and within the ice contributedled to overall higherelevated CT:AT ratios, resulting in higher pCO_2 and lower pH and Q Aragonite values in surface waters. There is evidence that once the sea ice melt facilitated bloom fully develops and CT is removed by PP from seawater by PP, higher pH and Q Aragonite values can be expected along the sea ice edge (Tynan et al., 2016). This can be seen process is reflected in the photic zone of station 15 at 32 m, where an oxygen maximum (and AOU minimum) was present, which indicates high PP, resulting in a pH maximum (8.20) and pCO_2 minimum (249 μ atm) (refer to Sect. 3.4).

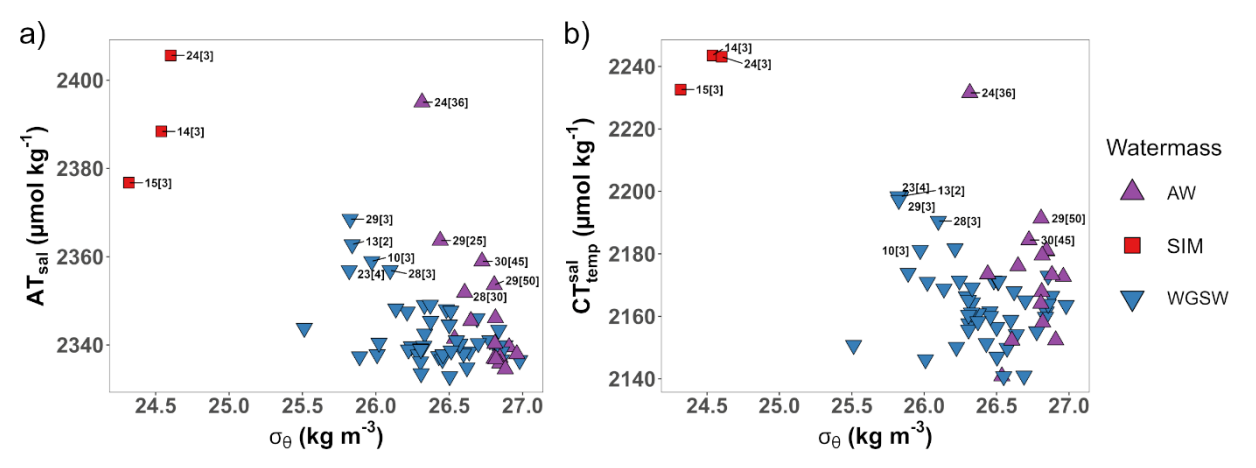


Figure 7: First 50 m of the water column for a) salinity-normalized AT values against pot. density and b) temperature-salinity-normalized CT values against pot. density. Different water mass categories are given in the legend. SIM affected stations (14, 15, 24) and stations adjacent to those (10, 13, 23, 28, 29, 30) are labeled. The number in brackets corresponds to the sampling depth.

We observed higher elevated surface water concentrations of dFe, dCo, dNi, dCu, and dCd in areas that were recently covered by sea ice, particulary towards the west of each transect (refer to Sect. 3.3). This observation aligns This ties in nicely with a study by Tovar-Sánchez et al. (2010), who observed an enrichment of these trace elements these trace elements to be enriched in sea ice relative to surface waters, suggesting that sea ice meltwater is a significant source of these trace elements to surface waters in Baffin Bay-surface waters. In particular Especially, the additional input of dFe from melting sea ice may play a biologically important role eould be biologically important in maintaining ice-edge blooms, as previously observed seen, e.g., in the Bering Sea (Aguilar-Islas et al., 2008). In addition to sea ice input Besides the additional input through sea ice meltwater, we suggest that, much likesimilar to macronutrients, trace elements had we not yet been removed from surface waters by biological uptake at the time of sampling. We hypothesize that following the development of after the occurrence of the bloom, concentrations of both macronutrients as well as and trace elements eoncentrations would declinerease, as already observed much like we already saw happening in surface waters at of shelf stations closer to the Greenlandic coast. Consistent with findings from other Arctic regions Similar to other regions of the Arctic (Kanna et al., 2014; Nakanowatari et al., 2007).

the progressive melting and retreat of sea ice <u>in Baffin Bay and Davis Strait appears to significantly influencealters</u> the biogeochemical cyclinges of carbon and trace elements, as well as the biological productivity in Baffin Bay and Davis Strait.

695 4.45 Influence of freshwater runoff from coastal sources on biogeochemical properties

700

705

710

715

720

The influence of coastal freshwater runoff on the chemical composition of surface waters was demonstrated throughdemonstraded by statistical analysis (refer to Sect. 4.1.2) and is evident in minimum salinity values (refer to Sect. 3.1) observed inat surface waters of stations 6, 11, and 17 (refer to Sect. 3.1). Stations 6 and 11 are located close-near to the mouths of the Kangerlussuaq Fjord and the Nassuttooq Fjord, both of which receive glacial and riverine freshwater draining from the GIS (Monteban et al., 2020). Station 17 is located in Disko Bay, approximately 70 km from the mouth of the Ilulissat Icefjord/Jakobshavn Isbræ system, where glacially modified waters form a buoyant coastal current outside the fjord (Beaird et al., 2017). These low-salinity surface waters Minimum salinity values in surface waters coincide with higher elevated macronutrient concentrations (refer to Sect. 3.2). A modeling study by Møller et al. (2023) has showndemonstrated that part a portion of the macronutrient input into Disko Bay is directly coupled linked to freshwater runoff-as a source. Other-Additional mechanisms that replenish-transport marine-sourced nutrients from deeper waters into the photic zone includeare vertical mixing fueled by wind and tide (Møller et al., 2023), as well as or via the estuarine upwelling circulation forced by the glacier's freshwater input (Williams et al., 2021). Our results suggest that the continued replenishment of macronutrients into the photic zone of Disko Bay can sustain PP into the summer season. This which is evidence devident by high oxygen and low AOU concentrations in surface waters atof station 17 (refer to Sect. 3.1). These conditions have significant implications This has large implications foron the carbonate system and the uptake of CO₂, which is as reflected by low Revelle factors and low pCO₂ values in surface waters of Disko Bay (refer to Sect. 3.4). A similar pattern was observed in the Godthåbsfjord system in southern Greenland, where biological processes were identified as the primary drivers of CO₂ uptake, resulting in low surface water pCO₂A similar observation for the Godthåbsfjord system in south Greenland revealed biological processes to be the most important drivers of CO₂ uptake, resulting in low pCO₂ concentrations in surface waters of the shelf area (Meire et al., 2015). Based on these findings and supporting literature, we propose that nutrient cycling in Disko Bay is strongly influenced by GIS-derived freshwater input. This input stimulates PP and establishes Disko Bay as an important seasonal sink for atmospheric CO₂ well into the summer. Our results highlight that nutrient cycling in Disko Bay is strongly driven by GISderived freshwater input, which stimulates PP and creates an important sink for CO2 long into the summer season. Apart from the Disko Bay area, the surface water of stations closest to the coast of Greenland were corrosive with lower buffering capacities (refer to Sect. 3.4). Apart from the Disko Bay area, surface waters at stations closest to the Greenland coast exhibited lower Ω Aragonite values with lower buffering capacities (refer to Sect. 3.4). Glacial freshwater discharge from the GIS is known to have a strong AT-dilution effect on AT relative to CT, which impacts reduces the buffering capacity of surface waters, resulting in lower Ω Aragonite saturation states and pH values (Henson et al., 2023; Burgers et al., 2024). However, The acidification of surface waters acidification can be mitigated by PP, which removes CT from the photic zone-, consequently increasing and thus increases both pH and Ω Aragonite (Chierici and Fransson, 2009), as seen observed infor the Disko Bay area. At coastal stations, surface waters Surface waters of coastal stations showed exhibited negative AOU values, indicating CT drawdown by via PP. Simultaneously, extremely low NOx values (< LOO) were detected present, suggesting that PP was approaching nutrient limitation was reaching a limit due to nutrient depletion. This nutrient depletion likely constrained further CT uptake, thereby no longer compensating the AT dilution effect caused by the GIS freshwater input. As a result, surface waters exhibited lower pH values coupled with higher Revelle factors and pCO₂ values. This could explain lower pH values coupled with higher Revelle factors and pCO2 values, as the AT dilution effect caused by the GIS freshwater input is no longer compensated for by CT removal through biological processes. Our findings suggest that as the summer season progresses and PP declines, surface waters along the west Greenland coast become increasingly vulnerable to acidification due to the input of poorly buffered glacial freshwater. Our results indicate that surface waters along west Greenland become more susceptible to acidification through the input of poorly buffered glacial freshwater as the summer season progresses and PP decreases. These observations are consistent Our results agree well with Henson et al. (2023), who observed that AT dilution from glacial meltwater to drives corrosive conditions in Greenlandic coastal surface waters of the Greenlandic coast, leading to a general decline in bothcausing an overall decrease in Ω Aragonite and pH (refer to Sect. 3.4). In addition to influencing the cycling of macronutrients and carbon Besides the cycling of macronutrients and carbon, coastal freshwater input significantly affects the distribution of trace elements the distribution of trace elements is influenced by coastal freshwater input. Overall, the sSurface water concentrations of dMn, dFe, dCo, dNi, and dCu were generally highest close to the coast and decreased with increasing distance along each transect. This trend was especially pronounced at For stations 11 and 12 (mouth of Nassuttooq Fjord), and as well as station 17 (Disko Bay, Ilulissat Icefjord) this trend was especially pronounced, reflecting-highlighting the influence of freshwater glacial runoff from the GIS, which introduces freshwater with a distinct chemical composition (refer to Sect. 4.2.3). Our work is consistent withconfirmed by previous findings studies from different various regions around Greenland, which have identified GIS-derived freshwater as a source of trace elements including that suggest the freshwater flux from the GIS to be a source of dMn, dFe, dCo, dNi, and dCu (Chen et al., 2022; Krause et al., 2021; Hawkings et al., 2020; Krisch et al., 2022a; Colombo et al., 2020). While Ssurface water concentrations of dNi in Disko Bay remained relatively constant, elevated concentrations were observed whereas stations at the mouth of Nassuttoog Fjord exhibited higher concentrations. Similar spatial variability in dNi has been reported A similar observation was done by Krause et al. (2021), who related varying dNithese trends along coastal transects to the presence of outcrops of Ni-rich minerals across-along the West Greenland coast. The input of bioactive trace elements, e.g., dMn, dFe, and dCo, via GIS freshwater runoff has been suggested to stimulate enhance primary productivity in the surrounding adjacent shelf areas (Bhatia et al., 2013; Hawkings et al., 2020). Our study provides further evidence that freshwater from the GIS could may support biological processes by supplying bioactive trace elements to surface waters.

730

735

740

745

750

755

5 Summary and Conclusion

760

765

770

775

780

785

highly dynamic and influenced by the complex interplay between physicochemical drivers, major ocean currents, sea ice melting, and terrestrial freshwater runoff from the GIS. The biogeochemical cycling of these parameters is governed by several key mechanisms. First, conservative mixing along the salinity gradient differentiates between fresher surface waters (WGSW, AW, SIM) and more saline, deeper waters (WGIW, TrW, BBW). While AT, CT, and dV show positive correlations with salinity due to dilution by freshwater, dCu shows a negative correlation, indicating coastal and sea ice meltwater as sources. Second, biological processes regulate the vertical fluxes of macronutrients, CT, and trace metals such as dFe, dNi, and dCd by photosynthetic uptake and OM remineralization. In the deep waters of Baffin Bay, the long residence time and the enclosed bathymetry promote the accumulation of remineralized nutrients and CT. This accumulation drives corrosive conditions, resulting in Ω Aragonite undersaturation in deep waters of southern Baffin Bay. Such conditions pose a potential threat to the benthic ecosystem of the west Greenland shelf, particularly by creating an unfavourable environment for shell-forming marine organisms. Third, benthic fluxes across the sediment-water interface contribute to elevated concentrations of certain trace elements (e.g., dMn, dFe, dCo, and dNi) in bottom waters of shelf stations. We hypothesize that the magnitude of this return flux decreases with increasing distance from the Greenlandic coast, likely due to reduced deposition of biogenic and terrigenous material available for remineralization and reversible scavenging. Further investigation of Baffin Bay sediments is necessary to quantify benthic fluxes of trace elements and geochemical reactions occurring within the sediment. Our study provides an initial assessment of the role of benthic inputs in trace element cycling on the west Greenland shelf and Baffin Bay, highlighting their potential significance in shaping regional biogeochemistry. The internal cycling of chemical constituents in the water column is driven by conservative mixing, with freshwater either being a source (dCu) or causing dilution (AT, CT, and dV) of parameter concentrations. Furthermore, we observed biological processes determining the pelagic flux of macronutrients, trace elements (dFe, dNi, and dCd) and carbonate system parameters. The long residence time of deep and bottom waters in Baffin Bay, along with an enclosed bathymetry that restricts circulation, facilitated the accumulation of remineralized nutrients and CT, which drove corrosive conditions and Q Aragonite undersaturation in deep waters of southern Baffin Bay. Thus, the benthic ecosystem of the west Greenland shelf is potentially vulnerable to future ocean acidification and suppression of CaCO₃ saturation states. The distribution of trace elements in the

The distribution of macronutrients, carbonate system species, and dissolved trace elements on the west Greenland shelf is

study area was diverse and depended on both the intrinsic chemical behavior of each element and extrinsic factors such as biological processes (uptake and remineralization) or local sources (e.g., coastal runoff, sea ice, benthic processes). We described conservative (dV, dCu), nutrient type (dFe, dNi, and dCd) and scavenged type (dMn, dFe, dCo, dNi, and dCu) profiles, which correspond well with previously published data in the Arctic. Additionally, an increase in dMn, dFe, dCo, and dNi concentrations was noticeable for deep water shelf stations, which we relate to benthic fluxes at the sediment water interface. We hypothesize that this return flux decreased with increasing distance from the Greenlandic coast as the amount of exported biogenic and terrigenous material available for remineralization and reversible scavenging also decreased. Further

studies looking into Baffin Bay sediments are needed to disclose benthic fluxes of trace elements and reactions occurring
therein. Our study provides a first insight into the importance of benthic inputs for trace element cycling on the west Greenland shelf and Baffin Bay.

795

800

805

810

815

820

The distribution of chemical constituents in the water column across the west Greenland shelf is primarily governed mainly influenced by the opposing directions of the BIC and the WGC and their respective water masses. The BIC transports the The southward-moving AW, which combines winter-cooled water in-from Baffin Bay with Pacific-origin Arctic Ocean water inflow of cold and fresh Arctic Ocean water of Pacific originentering-through the CAA. We characterized this water mass as cold and fresh, exhibiting highwith elevated nutrient contents concentrations and high CT:AT ratios, reflecting due to both the lower biological activity and the inflow of additional CT input transported throughfrom the CAA to Baffin Bay. Elevated concentrations of dFe, dMn, dCo, dNi, and dCu were present-observed in AW, likely due to the influence of trace elementrich outflows from the CAAbecause of the CAA outflow into Baffin Bay. In contrast, the northward moving WGSW, transported northward by the WGC, integrates freshwater of Arctic-origin from East Greenland that mixes with with glacial meltwater from the GIS. This water mass dominated the upper water column on the shelf and is characterized as warm and fresh, with high biological productivity and correspondingly low nutrient concentrations due to biological uptake., which we characterized as warm and fresh, highly productive, and therefore exhibiting low nutrient concentrations. Below-Beneath the WGSW lies the WGIW, a warm and salty WGIW, water mass which originates in theof North Atlantic origin. This water mass is enriched in nutrients and carbon due to the remineralization of OMis dominated by the remineralization of OM, leading to the enrichment of nutrients and carbon. The gradual mixing of these three water masses along the shelf was further illustrated by the latitudinal distribution of dPb, We described the gradual mixing of all three water masses along the shelf by using the latitudinal distribution of dPb, which is influenced by elevated dPb waters from the North Atlantic and low dPb waters from the CAA.

Our study provides evidence that the progressive melting and retreat of sea ice alters the biological productivity as well as and the biogeochemical cyclinges of carbon and trace elements in surface waters of southern Baffin Bay. The east-to-west direction retreat of sea ice retreat during spring and summer caused established a significant gradient in nutrient concentrations. Nutrients were lowest in the highly productive shelf waters along the eastern side of the west Greenland coast, while higher concentrations nutrients were observed higher towards the west of southern Baffin Bay, where sea ice cover persisted for a longer duration because of the prolonged sea ice cover. The timing of this study enabled us to capture the beginning onset of a phytoplankton bloom in areas that were previously covered by sea ice, but where nutrients had not yet been consumed depleted. Additionally, sea ice meltwater provided additional AT to surface waters, likely through the dissolution of ikaite. However, This small geochemical buffer was offset by the presence of excesselevated CT concentrations, potentially derived from organic carbon the remineralization of OM under and within the ice and the inflow of CT-rich Pacific-origin waters via the additional CT input through the CAA to Baffin Bay. Overall, the combined influence of sea ice meltwater and the inflow of Pacific-origin waters lowered reduced AT relative to CT, resulting in elevated and are responsible for higher-pCO₂ and lower-decreased pH and Ω Aragonite values in surface waters. As the ice-edge bloom progressesOnce the sea ice melt

facilitated bloom fully develops and CT is removed by PP, an increase inhigher pH and Ω Aragonite values can be expected along the retreating ice margineould be expected along the sea ice edge. Furthermore, we observed identified sea ice meltwater as a source of bioactive trace elements, including dFe, dCo, dNi, dCu, and dCd to surface waters of southern Baffin Bay-surface waters. This additional input of micronutrients may sustain As an additional source of bioactive trace elements, this could maintain and prolong the duration of ice-edge blooms, with implications for regional productivity and biogeochemical cycling. We observed that freshwater runoff from the GIS significantly influenceding the chemical composition of coastal waters along west Greenland, especially particularly in Disko Bay and at the mouth of the Nassuttooq Fjord. In the Disko Bay area, GIS-derived freshwater input replenished macronutrients in the photic zone, stimulating PP and creating an important sink for CO₂ long into the summer season. The supply of bioactive trace elements via GIS freshwater runoff, could further support biological processes in the surrounding shelf areas. However, in areas along the coastline coastal areas where PP approached nutrient limitationwas reaching a limit due to low nutrient concentrations, surface waters became more susceptible to acidification through due to the input of poorly buffered glacial freshwater.

This work successfully captured a high-resolution, large-scale snapshot of various water column parameters across the west Greenland shelf during July. Nevertheless However, we were not ableunable to resolve any seasonal variations variability, which requires observations at ean only be provided by time series studies higher temporal resolution. We emphasize the need for sustained time-series observations believe that higher temporal monitoring is necessary to fully assess the consequences of climate change in this climate-sensitive region.

Data availability statement

The data set for the carbonate system and dissolved trace elements can be found online at: https://doi.org/10.5281/zenodo.14235091 (Schmidt et al., 2024).

Supplement link

The supplements to this article can be found online at: XXX

Author contribution

Claudia-E.-Schmidt: Conceptualization, Formal Analysis, Investigation, Methodology, Data curation, Visualization, Writing – original draft

Tristan-Zimmermann: Writing – review & editing

850 Katarzyna Koziorowska Makuch: Investigation, Writing – review & editing

Daniel-Proefrock: Resources, Supervision, Writing – review & editing

Helmuth Thomas: Funding acquisition, Project administration, Resources, Writing – review & editing

Declaration of competing interest

The authors declare that they have no conflict of interest.

855 Acknowledgement

The authors would like to thank the captain and crew of RV Dana for their support during the sampling campaign in 2021. Special thanks to Camilla Svensen and Ulrike Dietrich (both University of Tromsø) for the collection of the nutrient samples and Colin Stedmon and his team (Technical University of Denmark) for the nutrient analysis.

Financial support

This project has received funding from the European Union's Horizon 2020 research and innovation program under Grant Agreement No. 869383 (ECOTIP) and the European Union's Horizon 2023 research and innovation program under Grant Agreement No. 101136480 (SEA-Quester). The project was made possible through the program "Changing Earth – Sustaining our Future" (Subtopic 4.1) within the Helmholtz Association.

References

880

885

890

- Aguilar-Islas, A. M., Rember, R. D., Mordy, C. W., and Wu, J.: Sea ice-derived dissolved iron and its potential influence on the spring algal bloom in the Bering Sea, Geophysical Research Letters, 35, doi:10.1029/2008GL035736, 2008.
 - Akima, H., and Gebhardt, A.: akima: Interpolation of Irregularly and Regularly Spaced Data, CRAN [code], https://CRAN.R-project.org/package=akima, 2022.
 - Aksenov, Y., Karcher, M., Proshutinsky, A., Gerdes, R., de Cuevas, B., Golubeva, E., Kauker, F., Nguyen, A. T., Platov, G.
- A., Wadley, M., Watanabe, E., Coward, A. C., and Nurser, A. J.: Arctic pathways of Pacific Water: Arctic Ocean Model Intercomparison experiments, Journal of geophysical research. Oceans, 121, 27-59, doi:10.1002/2015jc011299, 2016.
 - Arnone, V., Santana-Casiano, J. M., González-Dávila, M., Planquette, H., Sarthou, G., Gerringa, L. J. A., and González, A. G.: Natural copper-binding ligands in the Arctic Ocean. The influence of the Transpolar Drift (GEOTRACES GN04), Frontiers in Marine Science, 10, doi:10.3389/fmars.2023.1306278, 2023.
- Azetsu-Scott, K., Clarke, A., Falkner, K., Hamilton, J., Jones, E. P., Lee, C., Petrie, B., Prinsenberg, S., Starr, M., and Yeats, P.: Calcium carbonate saturation states in the waters of the Canadian Arctic Archipelago and the Labrador Sea, Journal of Geophysical Research: Oceans, 115, doi:10.1029/2009JC005917, 2010.
 - Ballinger, T. J., Moore, G. W. K., Garcia-Quintana, Y., Myers, P. G., Imrit, A. A., Topál, D., and Meier, W. N.: Abrupt Northern Baffin Bay Autumn Warming and Sea-Ice Loss Since the Turn of the Twenty-First Century, Geophysical Research Letters, 49, e2022GL101472, doi:10.1029/2022GL101472, 2022.
 - Bates, N. R., and Mathis, J. T.: The Arctic Ocean marine carbon cycle: evaluation of air-sea CO₂ exchanges, ocean acidification impacts and potential feedbacks, Biogeosciences, 6, 2433-2459, doi:10.5194/bg-6-2433-2009, 2009.
 - Bates, N. R., Mathis, J. T., and Cooper, L. W.: Ocean acidification and biologically induced seasonality of carbonate mineral saturation states in the western Arctic Ocean, Journal of Geophysical Research: Oceans, 114, doi:10.1029/2008JC004862, 2009.
 - Beaird, N., Straneo, F., and Jenkins, W.: Characteristics of meltwater export from Jakobshavn Isbræ and Ilulissat Icefjord, Annals of Glaciology, 58, 107-117, doi:10.1017/aog.2017.19, 2017.
 - Beaupré-Laperrière, A., Mucci, A., and Thomas, H.: The recent state and variability of the carbonate system of the Canadian Arctic Archipelago and adjacent basins in the context of ocean acidification, Biogeosciences, 17, 3923-3942, doi:10.5194/bg-17-3923-2020, 2020.
 - Bhatia, M. P., Kujawinski, E. B., Das, S. B., Breier, C. F., Henderson, P. B., and Charette, M. A.: Greenland meltwater as a significant and potentially bioavailable source of iron to the ocean, Nature Geoscience, 6, 274-278, doi:10.1038/ngeo1746, 2013.
- Bi, H., Zhang, Z., Wang, Y., Xu, X., Liang, Y., Huang, J., Liu, Y., and Fu, M.: Baffin Bay sea ice inflow and outflow: 1978–1979 to 2016–2017, The Cryosphere, 13, 1025-1042, doi:10.5194/tc-13-1025-2019, 2019.

- Bruyant, F., Amiraux, R., Amyot, M.-P., Archambault, P., Artigue, L., Barbedo de Freitas, L., Bécu, G., Bélanger, S., Bourgain, P., Bricaud, A., Brouard, E., Brunet, C., Burgers, T., Caleb, D., Chalut, K., Claustre, H., Cornet-Barthaux, V., Coupel, P., Cusa, M., Cusset, F., Dadaglio, L., Davelaar, M., Deslongchamps, G., Dimier, C., Dinasquet, J., Dumont, D., Else, B., Eulaers, I., Ferland, J., Filteau, G., Forget, M.-H., Fort, J., Fortier, L., Galí-Tapías, M., Gallinari, M., Garbus, S.-E., Garcia, N., Gérikas Ribeiro, C., Gombault, C., Gourvil, P., Goyens, C., Grant, C., Grondin, P.-L., Guillot, P., Hillion, S., Hussherr, R.,
- Joux, F., Joy-Warren, H., Joyal, G., Kieber, D., Lafond, A., Lagunas, J., Lajeunesse, P., Lalande, C., Larivière, J., Le Gall, F., Leblanc, K., Leblanc, M., Legras, J., Levesque, K., Lewis, K.-M., Leymarie, E., Leynaert, A., Linkowski, T., Lizotte, M., Lopes dos Santos, A., Marec, C., Marie, D., Massé, G., Massicotte, P., Matsuoka, A., Miller, L., Mirshak, S., Morata, N., Moriceau, B., Morin, P.-I., Morisset, S., Mosbech, A., Mucci, A., Nadaï, G., Nozais, C., Obernosterer, I., Paire, T.,
- Panagiotopoulos, C., Parenteau, M., Pelletier, N., Picheral, M., Quéguiner, B., Raimbault, P., Ras, J., Rehm, E., Ribot Lacosta, L., Rontani, J.-F., Saint-Béat, B., Sansoulet, J., Sardet, N., Schmechtig, C., Sciandra, A., Sempéré, R., Sévigny, C., Toullec, J., Tragin, M., Tremblay, J.-E., Trottier, A.-P., Vaulot, D., Vladoiu, A., Xue, L., Yunda-Guarin, G., and Babin, M.: The Green Edge cruise: following the evolution of the Arctic phytoplankton spring bloom, from ice-covered to open waters, SEANOE [data set], doi:10.17882/86417, 2022.
- Bundy, R. M., Tagliabue, A., Hawco, N. J., Morton, P. L., Twining, B. S., Hatta, M., Noble, A. E., Cape, M. R., John, S. G., Cullen, J. T., and Saito, M. A.: Elevated sources of cobalt in the Arctic Ocean, Biogeosciences, 17, 4745-4767, doi:10.5194/bg-17-4745-2020, 2020.
- Burgers, T. M., Azetsu-Scott, K., Myers, P. G., Else, B. G. T., Miller, L. A., Rysgaard, S., Chan, W., Tremblay, J.-É., and Papakyriakou, T.: Unraveling the Biogeochemical Drivers of Aragonite Saturation State in Baffin Bay: Insights From the West Greenland Continental Shelf, Journal of Geophysical Research: Oceans, 129, e2024JC021122, doi:10.1029/2024JC021122,

2024.

- Cape, M. R., Straneo, F., Beaird, N., Bundy, R. M., and Charette, M. A.: Nutrient release to oceans from buoyancy-driven upwelling at Greenland tidewater glaciers, Nature Geoscience, 12, 34-39, 10.1038/s41561-018-0268-4, 2019.
- Chen, X.-G., Krisch, S., Al-Hashem, A., Hopwood, M. J., Rutgers van der Loeff, M. M., Huhn, O., Lodeiro, P., Steffens, T., and Achterberg, E. P.: Dissolved, Labile, and Total Particulate Trace Metal Dynamics on the Northeast Greenland Shelf, Global Biogeochemical Cycles, 36, e2022GB007528, doi:10.1029/2022GB007528, 2022.
 - Chierici, M., and Fransson, A.: Calcium carbonate saturation in the surface water of the Arctic Ocean: undersaturation in freshwater influenced shelves, Biogeosciences, 6, 2421-2431, doi:10.5194/bg-6-2421-2009, 2009.
- Colombo, M., Rogalla, B., Myers, P. G., Allen, S. E., and Orians, K. J.: Tracing Dissolved Lead Sources in the Canadian 925 Arctic: Insights from the Canadian GEOTRACES Program, ACS Earth and Space Chemistry, 3, 1302-1314, doi:10.1021/acsearthspacechem.9b00083, 2019.
 - Colombo, M., Jackson, S. L., Cullen, J. T., and Orians, K. J.: Dissolved iron and manganese in the Canadian Arctic Ocean: On the biogeochemical processes controlling their distributions, Geochimica et Cosmochimica Acta, 277, 150-174, doi:10.1016/j.gca.2020.03.012, 2020.

- Olombo, M., Rogalla, B., Li, J., Allen, S. E., Orians, K. J., and Maldonado, M. T.: Canadian Arctic Archipelago Shelf-Ocean Interactions: A Major Iron Source to Pacific Derived Waters Transiting to the Atlantic, Global Biogeochemical Cycles, 35, e2021GB007058, doi:10.1029/2021GB007058, 2021.
 - Curry, B., Lee, C. M., and Petrie, B.: Volume, Freshwater, and Heat Fluxes through Davis Strait, 2004–05, Journal of Physical Oceanography, 41, 429-436, doi:10.1175/2010JPO4536.1, 2011.
- Curry, B., Lee, C. M., Petrie, B., Moritz, R. E., and Kwok, R.: Multiyear Volume, Liquid Freshwater, and Sea Ice Transports through Davis Strait, 2004–10, Journal of Physical Oceanography, 44, 1244-1266, doi:10.1175/JPO-D-13-0177.1, 2014.
 - Dickson, A. G., and Millero, F. J.: A comparison of the equilibrium constants for the dissociation of carbonic acid in seawater media, Deep Sea Research Part A. Oceanographic Research Papers, 34, 1733-1743, doi:10.1016/0198-0149(87)90021-5, 1987.
- Dickson, A. G.: Standard potential of the reaction: AgCl(s) + 12H2(g) = Ag(s) + HCl(aq), and and the standard acidity constant of the ion HSO4– in synthetic sea water from 273.15 to 318.15 K, The Journal of Chemical Thermodynamics, 22, 113-127,
- doi:10.1016/0021-9614(90)90074-Z, 1990.
 - DIN e.V.: DIN 32645: Chemical analysis—Decision limit, detection limit and determination limit under repeatability conditions—Terms, methods, evaluation, doi:10.31030/1465413, 2008.
- Ebeling, A., Zimmermann, T., Klein, O., Irrgeher, J., and Pröfrock, D.: Analysis of Seventeen Certified Water Reference 945 Materials for Trace and Technology-Critical Elements, Geostandards and Geoanalytical Research, 46, 351-378, doi:10.1111/ggr.12422, 2022.
 - Evans, L. K., and Nishioka, J.: Accumulation processes of trace metals into Arctic sea ice: distribution of Fe, Mn and Cd associated with ice structure, Marine Chemistry, 209, 36-47, doi:10.1016/j.marchem.2018.11.011, 2019.
- Finley, A., Banerjee, S., and Hjelle, Ø.: MBA: Multilevel B-Spline Approximation, CRAN [code], https://CRAN.R-950 project.org/package=MBA, 2022.
 - Foukal, N. P., and Pickart, R. S.: Moored Observations of the West Greenland Coastal Current along the Southwest Greenland Shelf, Journal of Physical Oceanography, 53, 2619-2632, doi:10.1175/JPO-D-23-0104.1, 2023.
 - Fransson, A., Chierici, M., Miller, L. A., Carnat, G., Shadwick, E., Thomas, H., Pineault, S., and Papakyriakou, T. N.: Impact of sea-ice processes on the carbonate system and ocean acidification at the ice-water interface of the Amundsen Gulf, Arctic
- Fransson, A., Chierici, M., Nomura, D., Granskog, M. A., Kristiansen, S., Martma, T., and Nehrke, G.: Effect of glacial drainage water on the CO2 system and ocean acidification state in an Arctic tidewater-glacier fjord during two contrasting years, Journal of Geophysical Research: Oceans, 120, 2413-2429, doi:10.1002/2014JC010320, 2015.

Ocean, Journal of Geophysical Research: Oceans, 118, 7001-7023, doi:10.1002/2013JC009164, 2013.

955

Fransson, A., Chierici, M., Granskog, M. A., Dodd, P. A., and Stedmon, C. A.: Impacts of glacial and sea-ice meltwater, primary production, and ocean CO2 uptake on ocean acidification state of waters by the 79 North Glacier and northeast Greenland shelf, Frontiers in Marine Science, Volume 10 - 2023, doi:10.3389/fmars.2023.1155126, 2023.

- GEBCO Bathymetric Compilation Group 2023: The GEBCO_2023 Grid a continuous terrain model of the global oceans and land, NERC EDS British Oceanographic Data Centre NOC [data set], doi:10.5285/f98b053b-0cbc-6c23-e053-6c86abc0af7b, 2023.
- GEOTRACES Intermediate Data Product Group: The GEOTRACES Intermediate Data Product 2021 version 2 (IDP2021v2), NERC EDS British Oceanographic Data Centre NOC [data set], doi:10.5285/ff46f034-f47c-05f9-e053-6c86abc0dc7e, 2023. Gerringa, L. J. A., Rijkenberg, M. J. A., Slagter, H. A., Laan, P., Paffrath, R., Bauch, D., Rutgers van der Loeff, M., and Middag, R.: Dissolved Cd, Co, Cu, Fe, Mn, Ni, and Zn in the Arctic Ocean, Journal of Geophysical Research: Oceans, 126, e2021JC017323, doi:10.1029/2021JC017323, 2021.
- Haine, T. W. N., Curry, B., Gerdes, R., Hansen, E., Karcher, M., Lee, C., Rudels, B., Spreen, G., de Steur, L., Stewart, K. D., and Woodgate, R.: Arctic freshwater export: Status, mechanisms, and prospects, Global and Planetary Change, 125, 13-35, doi:10.1016/j.gloplacha.2014.11.013, 2015.
 - Hansen, H. P., and Koroleff, F.: Determination of nutrients, in: Methods of Seawater Analysis, 159-228, doi:10.1002/9783527613984.ch10, 1999.
- Hawkings, J., Wadham, J., Tranter, M., Telling, J., Bagshaw, E., Beaton, A., Simmons, S.-L., Chandler, D., Tedstone, A., and Nienow, P.: The Greenland Ice Sheet as a hot spot of phosphorus weathering and export in the Arctic, Global Biogeochemical Cycles, 30, 191-210, doi:10.1002/2015GB005237, 2016.
 - Hawkings, J. R., Wadham, J. L., Tranter, M., Lawson, E., Sole, A., Cowton, T., Tedstone, A. J., Bartholomew, I., Nienow, P., Chandler, D., and Telling, J.: The effect of warming climate on nutrient and solute export from the Greenland Ice Sheet,
- 980 Geochemical Perspectives Letters, 1, 94-104, doi:10.7185/geochemlet.1510, 2015.
 - Hawkings, J. R., Wadham, J., Benning, L., Hendry, K., Tranter, M., Tedstone, A., Nienow, P., and Raiswell, R.: Ice sheets as a missing source of silica to the polar oceans, Nature Communications, 8, 14198, doi:10.1038/ncomms14198, 2017.
 - Hawkings, J. R., Skidmore, M. L., Wadham, J. L., Priscu, J. C., Morton, P. L., Hatton, J. E., Gardner, C. B., Kohler, T. J., Stibal, M., Bagshaw, E. A., Steigmeyer, A., Barker, J., Dore, J. E., Lyons, W. B., Tranter, M., and Spencer, R. G. M.: Enhanced
- trace element mobilization by Earth's ice sheets, Proceedings of the National Academy of Sciences, 117, 31648-31659, doi:10.1073/pnas.2014378117, 2020.
 - Hendry, K. R., Huvenne, V. A. I., Robinson, L. F., Annett, A., Badger, M., Jacobel, A. W., Ng, H. C., Opher, J., Pickering, R. A., Taylor, M. L., Bates, S. L., Cooper, A., Cushman, G. G., Goodwin, C., Hoy, S., Rowland, G., Samperiz, A., Williams, J. A., Achterberg, E. P., Arrowsmith, C., Alexander Brearley, J., Henley, S. F., Krause, J. W., Leng, M. J., Li, T., McManus, J.
- 990 F., Meredith, M. P., Perkins, R., and Woodward, E. M. S.: The biogeochemical impact of glacial meltwater from Southwest Greenland, Progress in Oceanography, 176, 102126, doi:10.1016/j.pocean.2019.102126, 2019.
 - Henson, H. C., Holding, J. M., Meire, L., Rysgaard, S., Stedmon, C. A., Stuart-Lee, A., Bendtsen, J., and Sejr, M.: Coastal freshening drives acidification state in Greenland fjords, Science of The Total Environment, 855, 158962, doi:10.1016/j.scitotenv.2022.158962, 2023.

- Hölemann, J. A., Schirmacher, M., and Prange, A.: Dissolved and Particulate Major and Trace Elements in Newly Formed Ice 995 from the Laptev Sea (Transdrift III, October 1995), in: Land-Ocean Systems in the Siberian Arctic: Dynamics and History, edited by: Kassens, H., Bauch, H. A., Dmitrenko, I. A., Eicken, H., Hubberten, H.-W., Melles, M., Thiede, J., and Timokhov, L. A., Springer Berlin Heidelberg, Berlin, Heidelberg, 101-111, doi:10.1007/978-3-642-60134-7 11, 1999.
- 1000 Carlson, D. F., Chierici, M., Clarke, J. S., Cozzi, S., Fransson, A., Juul-Pedersen, T., Winding, M. H. S., and Meire, L.: Review article: How does glacier discharge affect marine biogeochemistry and primary production in the Arctic?, The Cryosphere, 14, 1347-1383, doi:10.5194/tc-14-1347-2020, 2020.
 - Jensen, L. T., Cullen, J. T., Jackson, S. L., Gerringa, L. J. A., Bauch, D., Middag, R., Sherrell, R. M., and Fitzsimmons, J. N.: A Refinement of the Processes Controlling Dissolved Copper and Nickel Biogeochemistry: Insights From the Pan-Arctic,

Hopwood, M. J., Carroll, D., Dunse, T., Hodson, A., Holding, J. M., Iriarte, J. L., Ribeiro, S., Achterberg, E. P., Cantoni, C.,

Journal of Geophysical Research: Oceans, 127, e2021JC018087, doi:10.1029/2021JC018087, 2022. Jones, E. M., Chierici, M., Menze, S., Fransson, A., Ingvaldsen, R. B., and Lødemel, H. H.: Ocean acidification state variability the Atlantic Arctic Ocean around northern Svalbard. **Progress** in Oceanography. 199. 102708. of doi:10.1016/j.pocean.2021.102708, 2021.

1005

- Jones, E. P., Coote, A. R., and Levy, E. M.: Effect of sea ice meltwater on the alkalinity of seawater, ISSN: 0022-2402, 1983.
- 1010 Juranek, L.: Changing Biogeochemistry of the Arctic Ocean: Surface Nutrient and CO2 Cycling in a Warming, Melting North, Oceanography, doi:10.5670/oceanog.2022.120, 2022.
 - Juul-Pedersen, T., Arendt, K. E., Mortensen, J., Blicher, M. E., Søgaard, D. H., and Rysgaard, S.: Seasonal and interannual phytoplankton production in a sub-Arctic tidewater outlet glacier fjord, SW Greenland, Marine Ecology Progress Series, 524, 27-38, https://www.int-res.com/abstracts/meps/v524/p27-38/, 2015.
- 1015 Kanna, N., Toyota, T., and Nishioka, J.: Iron and macro-nutrient concentrations in sea ice and their impact on the nutritional status of surface waters in the southern Okhotsk Sea. Progress in Oceanography, 126. 44-57. doi:10.1016/j.pocean.2014.04.012, 2014.
 - Krause, J., Hopwood, M. J., Höfer, J., Krisch, S., Achterberg, E. P., Alarcón, E., Carroll, D., González, H. E., Juul-Pedersen, T., Liu, T., Lodeiro, P., Meire, L., and Rosing, M. T.: Trace Element (Fe, Co, Ni and Cu) Dynamics Across the Salinity
- 1020 Gradient in Arctic and Antarctic Glacier Fjords, Frontiers in Earth Science, 9, doi:10.3389/feart.2021.725279, 2021. Krawczyk, D. W., Kryk, A., Juggins, S., Burmeister, A., Pearce, C., Seidenkrantz, M. S., Moros, M., Høyer, J. L., Kuijpers, A., and Witkowski, A.: Spatio-temporal changes in ocean conditions and primary production in Baffin Bay and the Labrador Sea, Palaeogeography, Palaeoclimatology, Palaeoecology, 563, 110175, doi:10.1016/j.palaeo.2020.110175, 2021.
 - Krisch, S., Hopwood, M. J., Roig, S., Gerringa, L. J. A., Middag, R., Rutgers van der Loeff, M. M., Petrova, M. V., Lodeiro,
- 1025 P., Colombo, M., Cullen, J. T., Jackson, S. L., Heimbürger-Boavida, L.-E., and Achterberg, E. P.: Arctic – Atlantic Exchange of the Dissolved Micronutrients Iron, Manganese, Cobalt, Nickel, Copper and Zinc With a Focus on Fram Strait, Global Biogeochemical Cycles, 36, e2021GB007191, doi:10.1029/2021GB007191, 2022a.

- Krisch, S., Huhn, O., Al-Hashem, A., Hopwood, M. J., Lodeiro, P., and Achterberg, E. P.: Quantifying Ice-Sheet Derived Lead (Pb) Fluxes to the Ocean; A Case Study at Nioghalvfjerdsbræ, Geophysical Research Letters, 49, e2022GL100296, doi:10.1029/2022GL100296, 2022b.
- Lafond, A., Leblanc, K., Queguiner, B., Moriceau, B., Leynaert, A., Cornet, V., Legras, J., Ras, J., Parenteau, M., Garcia, N., Babin, M., and Tremblay, J.-E.: Late spring bloom development of pelagic diatoms in Baffin Bay, Elementa-science Of The Anthropocene, 7, doi:10.1525/elementa.382, 2019.
 - Lehmann, N., Kienast, M., Granger, J., Bourbonnais, A., Altabet, M. A., and Tremblay, J.-É.: Remote Western Arctic Nutrients
- Fuel Remineralization in Deep Baffin Bay, Global Biogeochemical Cycles, 33, 649-667, doi:10.1029/2018GB006134, 2019. Li, Y.-H., and Tsui, T.-F.: The solubility of CO2 in water and sea water, Journal of Geophysical Research (1896-1977), 76, 4203-4207, doi:10.1029/JC076i018p04203, 1971.
 - Marsay, C. M., Aguilar-Islas, A., Fitzsimmons, J. N., Hatta, M., Jensen, L. T., John, S. G., Kadko, D., Landing, W. M., Lanning, N. T., Morton, P. L., Pasqualini, A., Rauschenberg, S., Sherrell, R. M., Shiller, A. M., Twining, B. S., Whitmore, L.
- M., Zhang, R., and Buck, C. S.: Dissolved and particulate trace elements in late summer Arctic melt ponds, Marine Chemistry, 204, 70-85, doi:10.1016/j.marchem.2018.06.002, 2018.
 - McConnell, J. R., and Edwards, R.: Coal burning leaves toxic heavy metal legacy in the Arctic, Proceedings of the National Academy of Sciences, 105, 12140-12144, doi:10.1073/pnas.0803564105, 2008.
- Measures, C. I.: The role of entrained sediments in sea ice in the distribution of aluminium and iron in the surface waters of the Arctic Ocean, Marine Chemistry, 68, 59-70, doi:10.1016/S0304-4203(99)00065-1, 1999.
 - Mehrbach, C., Culberson, C. H., Hawley, J. E., and Pytkowicx, R. M.: MEASUREMENT OF THE APPARENT DISSOCIATION CONSTANTS OF CARBONIC ACID IN SEAWATER AT ATMOSPHERIC PRESSURE1, Limnology and Oceanography, 18, 897-907, doi:10.4319/lo.1973.18.6.0897, 1973.
 - Meire, L., Søgaard, D. H., Mortensen, J., Meysman, F. J. R., Soetaert, K., Arendt, K. E., Juul-Pedersen, T., Blicher, M. E., and
- Rysgaard, S.: Glacial meltwater and primary production are drivers of strong CO₂ uptake in fjord and coastal waters adjacent to the Greenland Ice Sheet, Biogeosciences, 12, 2347-2363, doi:10.5194/bg-12-2347-2015, 2015.
 - Meire, L., Mortensen, J., Meire, P., Juul-Pedersen, T., Sejr, M. K., Rysgaard, S., Nygaard, R., Huybrechts, P., and Meysman, F. J. R.: Marine-terminating glaciers sustain high productivity in Greenland fjords, Glob Chang Biol, 23, 5344-5357, doi:10.1111/gcb.13801, 2017.
- Miller, L., Davelaar, M., Caleb, D., Mucci, A., Burgers, T., Ahmed, M., and Irish, V.: Dissolved inorganic carbon (DIC), total alkalinity, stable oxygen isotope (O-18), temperature, salinity, dissolved oxygen and other parameters measured from discrete samples and profile observations during the Canadian Coast Guard Ship Amundsen ArcticNet cruise (EXPOCODE 18DL20160603, Leg 1 and Leg 2) in the Eastern Canadian Arctic, Baffin Bay, Nares Strait, Lancaster Sound, Barrow Strait and Coronation Gulf from 2016-06-03 to 2016-08-23 (NCEI Accession 0217304), NOAA National Centers for Environmental Information [data set], doi:10.25921/719e-qr37, 2020.

- Møller, E. F., Christensen, A., Larsen, J., Mankoff, K. D., Ribergaard, M. H., Sejr, M., Wallhead, P., and Maar, M.: The sensitivity of primary productivity in Disko Bay, a coastal Arctic ecosystem, to changes in freshwater discharge and sea ice cover, Ocean Sci., 19, 403-420, doi:10.5194/os-19-403-2023, 2023.
- Monteban, D., Pedersen, J. O. P., and Nielsen, M. H.: Physical oceanographic conditions and a sensitivity study on meltwater runoff in a West Greenland fjord: Kangerlussuaq, Oceanologia, 62, 460-477, doi:10.1016/j.oceano.2020.06.001, 2020.
 - Mouginot, J., Rignot, E., Bjørk, A. A., van den Broeke, M., Millan, R., Morlighem, M., Noël, B., Scheuchl, B., and Wood, M.: Forty-six years of Greenland Ice Sheet mass balance from 1972 to 2018, Proceedings of the National Academy of Sciences, 116, 9239-9244, doi:10.1073/pnas.1904242116, 2019.
- Nakanowatari, T., Ohshima, K. I., and Wakatsuchi, M.: Warming and oxygen decrease of intermediate water in the northwestern North Pacific, originating from the Sea of Okhotsk, 1955–2004, Geophysical Research Letters, 34, doi:10.1029/2006GL028243, 2007.
 - Niebauer, H. J., Alexander, V., and Henrichs, S. M.: A time-series study of the spring bloom at the Bering Sea ice edge I. Physical processes, chlorophyll and nutrient chemistry, Continental Shelf Research, 15, 1859-1877, doi:10.1016/0278-4343(94)00097-7, 1995.
- Oksman, M., Kvorning, A. B., Larsen, S. H., Kjeldsen, K. K., Mankoff, K. D., Colgan, W., Andersen, T. J., Nørgaard-Pedersen, N., Seidenkrantz, M. S., Mikkelsen, N., and Ribeiro, S.: Impact of freshwater runoff from the southwest Greenland Ice Sheet on fjord productivity since the late 19th century, The Cryosphere, 16, 2471-2491, doi:10.5194/tc-16-2471-2022, 2022. Perrette, M., Yool, A., Quartly, G. D., and Popova, E. E.: Near-ubiquity of ice-edge blooms in the Arctic, Biogeosciences, 8, 515-524, doi:10.5194/bg-8-515-2011, 2011.
- Pierrot, D., Wallace, D., and Lewis, E.: MS Excel program developed for CO2 system calculations, Carbon Dioxide Information Analysis Center [code], doi:10.3334/CDIAC/otg.CO2SYS_XLS_CDIAC105a, 2011.
 Posit team: RStudio: Integrated Development Environment for R, Posit Software, PBC [code], http://www.posit.co/, 2023.
 Przibilla, A., Iwainski, S., Zimmermann, T., and Pröfrock, D.: Impact of storage temperature and filtration method on dissolved trace metal concentrations in coastal water samples, Water Environment Research, 95, e10922, doi:10.1002/wer.10922, 2023.
- 1085 R Core Team: R: A Language and Environment for Statistical Computing, R Foundation for Statistical Computing [code], https://www.R-project.org/, 2022.
 - Revelle, W.: psych: Procedures for Psychological, Psychometric, and Personality Research, CRAN [code], https://CRAN.R-project.org/package=psych, 2024.
- Ruacho, A., Richon, C., Whitby, H., and Bundy, R. M.: Sources, sinks, and cycling of dissolved organic copper binding ligands in the ocean, Communications Earth & Environment, 3, 263, doi:10.1038/s43247-022-00597-1, 2022.
 - Rysgaard, S., Bendtsen, J., Delille, B., Dieckmann, G. S., Glud, R. N., Kennedy, H., Mortensen, J., Papadimitriou, S., Thomas, D. N., and Tison, J.-L.: Sea ice contribution to the air—sea CO₂ exchange in the Arctic and Southern Oceans, Tellus B: Chemical and Physical Meteorology, doi:10.1111/j.1600-0889.2011.00571.x, 2011.

- Rysgaard, S., Glud, R. N., Lennert, K., Cooper, M., Halden, N., Leakey, R. J. G., Hawthorne, F. C., and Barber, D.: Ikaite crystals in melting sea ice implications for CO₂ and pH levels in Arctic surface waters, The Cryosphere, 6, 901-908, doi:10.5194/tc-6-901-2012, 2012.
 - Sarmiento, J. L., and Gruber, N.: Ocean Biogeochemical Dynamics, Princeton University Press, ISBN: 9780691017075, 2006. Schmidt, C. E., Pröfrock, D., and Thomas, H.: ECOTIP Dana Cruise July 2021 Alkalinity (AT), dissolved inorganic carbon (CT) and dissolved trace elements, Zenodo [data set], doi:10.5281/zenodo.14235091, 2024.
- 1100 Schnetger, B., and Lehners, C.: Determination of nitrate plus nitrite in small volume marine water samples using vanadium(III)chloride as a reduction agent, Marine Chemistry, 160, 91-98, doi:10.1016/j.marchem.2014.01.010, 2014. Seo, H., Kim, G., Kim, T., Kim, I., Ra, K., and Jeong, H.: Trace elements (Fe, Mn, Co, Cu, Cd, and Ni) in the East Sea (Japan Sea): Distributions. boundary inputs. and scavenging processes. Marine Chemistry. 239. 104070. doi:10.1016/j.marchem.2021.104070, 2022.
- Shadwick, E. H., Thomas, H., Chierici, M., Else, B., Fransson, A., Michel, C., Miller, L. A., Mucci, A., Niemi, A., Papakyriakou, T. N., and Tremblay, J.-É.: Seasonal variability of the inorganic carbon system in the Amundsen Gulf region of the southeastern Beaufort Sea, Limnology and Oceanography, 56, 303-322, doi:10.4319/lo.2011.56.1.0303, 2011a.
 Shadwick, E. H., Thomas, H., Gratton, Y., Leong, D., Moore, S. A., Papakyriakou, T., and Prowe, A. E. F.: Export of Pacific carbon through the Arctic Archipelago to the North Atlantic, Continental Shelf Research, 31, 806-816, doi:10.1016/j.csr.2011.01.014, 2011b.
 - Shadwick, E. H., Trull, T. W., Thomas, H., and Gibson, J. A. E.: Vulnerability of Polar Oceans to Anthropogenic Acidification: Comparison of Arctic and Antarctic Seasonal Cycles, Scientific Reports, 3, 2339, doi:10.1038/srep02339, 2013.
 - Sherwood, O. A., Davin, S. H., Lehmann, N., Buchwald, C., Edinger, E. N., Lehmann, M. F., and Kienast, M.: Stable isotope ratios in seawater nitrate reflect the influence of Pacific water along the northwest Atlantic margin, Biogeosciences, 18, 4491-

1115

4510, doi:10.5194/bg-18-4491-2021, 2021.

- Smrzka, D., Zwicker, J., Bach, W., Feng, D., Himmler, T., Chen, D., and Peckmann, J.: The behavior of trace elements in seawater, sedimentary pore water, and their incorporation into carbonate minerals: a review, Facies, 65, 41, doi:10.1007/s10347-019-0581-4, 2019.
- Spreen, G., Kaleschke, L., and Heygster, G.: Sea ice remote sensing using AMSR-E 89-GHz channels, Journal of Geophysical Research: Oceans, 113, doi:10.1029/2005JC003384, 2008.
 - Strass, V. H., and Nöthig, E. M.: Seasonal shifts in ice edge phytoplankton blooms in the Barents Sea related to the water column stability, Polar Biology, 16, 409-422, doi:10.1007/BF02390423, 1996.
 - Stroeve, J., and Notz, D.: Changing state of Arctic sea ice across all seasons, Environmental Research Letters, 13, 103001, doi:10.1088/1748-9326/aade56, 2018.
- Tang, C. C. L., Ross, C. K., Yao, T., Petrie, B., DeTracey, B. M., and Dunlap, E.: The circulation, water masses and sea-ice of Baffin Bay, Progress in Oceanography, 63, 183-228, doi:10.1016/j.pocean.2004.09.005, 2004.

- Tovar-Sánchez, A., Duarte, C. M., Alonso, J. C., Lacorte, S., Tauler, R., and Galbán-Malagón, C.: Impacts of metals and nutrients released from melting multiyear Arctic sea ice, Journal of Geophysical Research: Oceans, 115, doi:10.1029/2009JC005685, 2010.
- 1130 Tremblay, J.-É., Gratton, Y., Carmack, E. C., Payne, C. D., and Price, N. M.: Impact of the large-scale Arctic circulation and the North Water Polynya on nutrient inventories in Baffin Bay, Journal of Geophysical Research: Oceans, 107, 26-21-26-14, doi:10.1029/2000JC000595, 2002.
 - Tynan, E., Clarke, J. S., Humphreys, M. P., Ribas-Ribas, M., Esposito, M., Rérolle, V. M. C., Schlosser, C., Thorpe, S. E., Tyrrell, T., and Achterberg, E. P.: Physical and biogeochemical controls on the variability in surface pH and calcium carbonate
- saturation states in the Atlantic sectors of the Arctic and Southern Oceans, Deep Sea Research Part II: Topical Studies in Oceanography, 127, 7-27, doi:10.1016/j.dsr2.2016.01.001, 2016.
 - Vancoppenolle, M., Meiners, K. M., Michel, C., Bopp, L., Brabant, F., Carnat, G., Delille, B., Lannuzel, D., Madec, G., Moreau, S., Tison, J.-L., and van der Merwe, P.: Role of sea ice in global biogeochemical cycles: emerging views and challenges, Quaternary Science Reviews, 79, 207-230, doi:10.1016/j.quascirev.2013.04.011, 2013
- Vernet, M., Ellingsen, I., Marchese, C., Bélanger, S., Cape, M., Slagstad, D., and Matrai, P. A.: Spatial variability in rates of net primary production (NPP) and onset of the spring bloom in Greenland shelf waters, Progress in Oceanography, 198, 102655, doi:10.1016/j.pocean.2021.102655, 2021.
- Vieira, L. H., Achterberg, E. P., Scholten, J., Beck, A. J., Liebetrau, V., Mills, M. M., and Arrigo, K. R.: Benthic fluxes of trace metals in the Chukchi Sea and their transport into the Arctic Ocean, Marine Chemistry, 208, 43-55, doi:10.1016/j.marchem.2018.11.001, 2019.
 - Whitmore, L. M., Morton, P. L., Twining, B. S., and Shiller, A. M.: Vanadium cycling in the Western Arctic Ocean is influenced by shelf-basin connectivity, Marine Chemistry, 216, 103701, doi:10.1016/j.marchem.2019.103701, 2019.
 - Williams, P. L., Burgess, D. O., Waterman, S., Roberts, M., Bertrand, E. M., and Bhatia, M. P.: Nutrient and Carbon Export From a Tidewater Glacier to the Coastal Ocean in the Canadian Arctic Archipelago, Journal of Geophysical Research: Biogeosciences, 126, e2021JG006289, doi:10.1029/2021JG006289, 2021.
 - Wouters, B., and Sasgen, I.: Increasing freshwater fluxes from the Greenland Ice Sheet observed from space, Oceanography, 35, 103-105, doi:10.5670/oceanog.2022.125, 2022.

1150

1155

Wu, Y., Hain, M. P., Humphreys, M. P., Hartman, S., and Tyrrell, T.: What drives the latitudinal gradient in open-ocean surface dissolved inorganic carbon concentration?, Biogeosciences, 16, 2661-2681, doi:10.5194/bg-16-2661-2019, 2019.